The microtubule end-binding protein EB2 is a central regulator of microtubule reorganisation in apico-basal epithelial differentiation

Deborah A. Goldspink[1], Jonathan R. Gadsby[1], Gemma Bellett[1], Jennifer Keynton[1], Benjamin J. Tyrrell[1], Elizabeth K. Lund[1], Penny P. Powell[2], Paul Thomas[1] and Mette M. Mogensen[1,*]

[1]School of Biological Sciences, University of East Anglia, Norwich Research Park, Norwich, NR4 7TJ, UK
[2]Norwich Medical School, University of East Anglia, Norwich Research Park, Norwich, NR4 7TJ, UK

*Author for correspondence (m.mogensen@uea.ac.uk)

Accepted 31 May 2013
Journal of Cell Science 126, 4000–4014

doi: 10.1242/jcs.129759

Summary

Microtubule end-binding (EB) proteins influence microtubule dynamic instability, a process that is essential for microtubule reorganisation during apico-basal epithelial differentiation. Here, we establish for the first time that expression of EB2, but not that of EB1, is crucial for initial microtubule reorganisation during apico-basal epithelial differentiation, and that EB2 downregulation promotes bundle formation. EB2 siRNA knockdown during early stages of apico-basal differentiation prevented microtubule reorganisation, whereas its downregulation at later stages promoted microtubule stability and bundle formation. Interestingly, although EB1 is not essential for microtubule reorganisation, its knockdown prevented apico-basal bundle formation and epithelial elongation. siRNA depletion of EB2 in undifferentiated epithelial cells induced the formation of straight, less dynamic microtubules with EB1 and ACF7 lattice association and co-alignment with actin filaments, a phenotype that could be rescued by inhibition with formin. Importantly, *in situ* inner ear and intestinal crypt epithelial tissue revealed direct correlations between a low level of EB2 expression and the presence of apico-basal microtubule bundles, which were absent where EB2 was elevated. EB2 is evidently important for initial microtubule reorganisation during epithelial polarisation, whereas its downregulation facilitates EB1 and ACF7 microtubule lattice association, microtubule-actin filament co-alignment and bundle formation. The spatiotemporal expression of EB2 thus dramatically influences microtubule organisation, EB1 and ACF7 deployment and epithelial differentiation.

Key words: EB2, EB1, ACF7, Epithelia, Microtubules, Cochlea, Intestinal crypt, Actin filaments

Introduction

Microtubule reorganisation is critical for differentiation, tissue formation and function and this is particularly evident during apico-basal polarisation of epithelial cells such as those of the kidney, intestine and inner ear. A radial microtubule array focused on a centrally located centrosome is typical of many undifferentiated epithelial cells. Here the microtubule minus-ends are anchored at the centrosome and the plus-ends extend towards the cell cortex. Cell-to-cell contact and polarisation trigger a dramatic reorganisation of these microtubules leading to the formation of an apico-basal array no longer anchored at the centrosome. The minus-ends of the apico-basal microtubules become anchored at apical, non-centrosomal sites associated with adherens junctions (Bacallao et al., 1989; Bellett et al., 2009; Mogensen et al., 2002; Moss et al., 2007). Evidence based on both *in situ* inner ear epithelial cells and *in vitro* cultures of Madin-Darby canine kidney (MDCKII) cells show that the microtubules of the apico-basal arrays originate from the centrosome but how they are subsequently reorganised remains to be determined (Bellett et al., 2009; Gierke and Wittmann, 2012).

EB1 is often referred to as the master controller of plus-end tracking proteins (+TIPs) being able to track the plus-end of growing microtubules and interact with most other +TIPs (Lansbergen and Akhmanova, 2006; Morrison et al., 1998). EB1 is evolutionary conserved, and three family members EB1, EB2 and EB3, encoded by separate (MAPRE) genes, are expressed in mammalian cells (Bu and Su, 2003; Su et al., 1995; Su and Qi, 2001). EB1 and EB3 influence microtubule dynamics by promoting growth and suppressing catastrophe whereas EB2 apparently does not (Komarova et al., 2009; Li et al., 2011; Tirnauer and Bierer, 2000; van der Vaart et al., 2009). However, relatively little is known about EB2's function in cells. EBs form dimers and bind microtubules via their N-terminal calponin homology (CH) domain and recent evidence suggest that tip recognition is due to a high affinity for GTP–tubulin, which is prominent at the growing end of microtubules (Dimitrov et al., 2008; Maurer et al., 2011; Maurer et al., 2012). Repulsive forces between the negatively charged C-terminus and the microtubule lattice are also likely to contribute to the plus-end localisation (Buey et al., 2011). EB1 and EB3, but to a lesser extent EB2, interact via the C-terminus with most other +TIPs including APC (adenomatous polyposis coli), CLIPs (cytoplasmic linker proteins), CLASPs (CLIP-associated proteins) and the microtubule-actin cross-linking spectraplakin ACF7 (MACF1). Hence, they regulate interactions of microtubules with the cell cortex, actin filaments, kinetochores and organelles (Kodama et al., 2003; Komarova et al., 2005; Lansbergen and Akhmanova, 2006; Wu et al., 2008). EBs may

thus influence microtubule reorganisation by regulating their dynamics and ability to interact with other structures.

Microtubule reorganisation and generation of apico-basal bundles is also likely to involve cytoskeletal cross-talk. The Rho GTPases are key regulators of the microtubule and actin cytoskeleton. They both regulate and are regulated by microtubule dynamics and control actin filament assembly and organisation. Microtubule depolymerisation by Nocodazole, for example, activates RhoA/ROCK and destabilises microtubules due to release of the Rho effector GEF-H1 from microtubules. RhoA/ROCK inhibition, on the other hand, induces microtubule stability and bundle formation as well as reducing stress fibres (Chang et al., 2008; Cheng et al., 2012; Gao et al., 2004; Kadir et al., 2011; Krendel et al., 2002; Scaife et al., 2003; Takesono et al., 2010).

Skeletal muscle, like differentiation of epithelial cells involves a major reorganisation of the microtubule network transforming the radial array of myoblasts into non-centrosomal parallel bundles in differentiated myotubes (Tassin et al., 1985). Intriguingly, a marked downregulation in EB2 expression has been reported during muscle differentiation while EB1 levels remained constant (Straube and Merdes, 2007). This suggests that downregulation of EB2 may be a prerequisite for microtubule bundle formation. We therefore focused our investigation on the role of EB2 in microtubule reorganisation and apico-basal bundle formation during epithelial differentiation.

Here we establish for the first time a role for EB2 in microtubule reorganisation during apico-basal epithelial differentiation. We report that EB2, but not EB1, expression is critical for microtubule reorganisation during early stages of epithelial differentiation whereas EB1 is important for apico-basal microtubule bundle formation and epithelial elongation. EB2 downregulation during latter stages of differentiation facilitates EB1 lattice association, ACF7 recruitment and microtubule-actin filament co-alignment and bundle formation. Furthermore, inhibition of the formin FH2 domain with SMIFH2 in EB2-depleted cells rescues the control phenotype.

Results

EB2 is expressed during early stages of apico-basal epithelial differentiation but downregulated in most cells at later stages

Mouse inner medullary kidney (mIMCD-3) cells were grown for 9 days resulting in highly confluent (partially polarised) epithelial

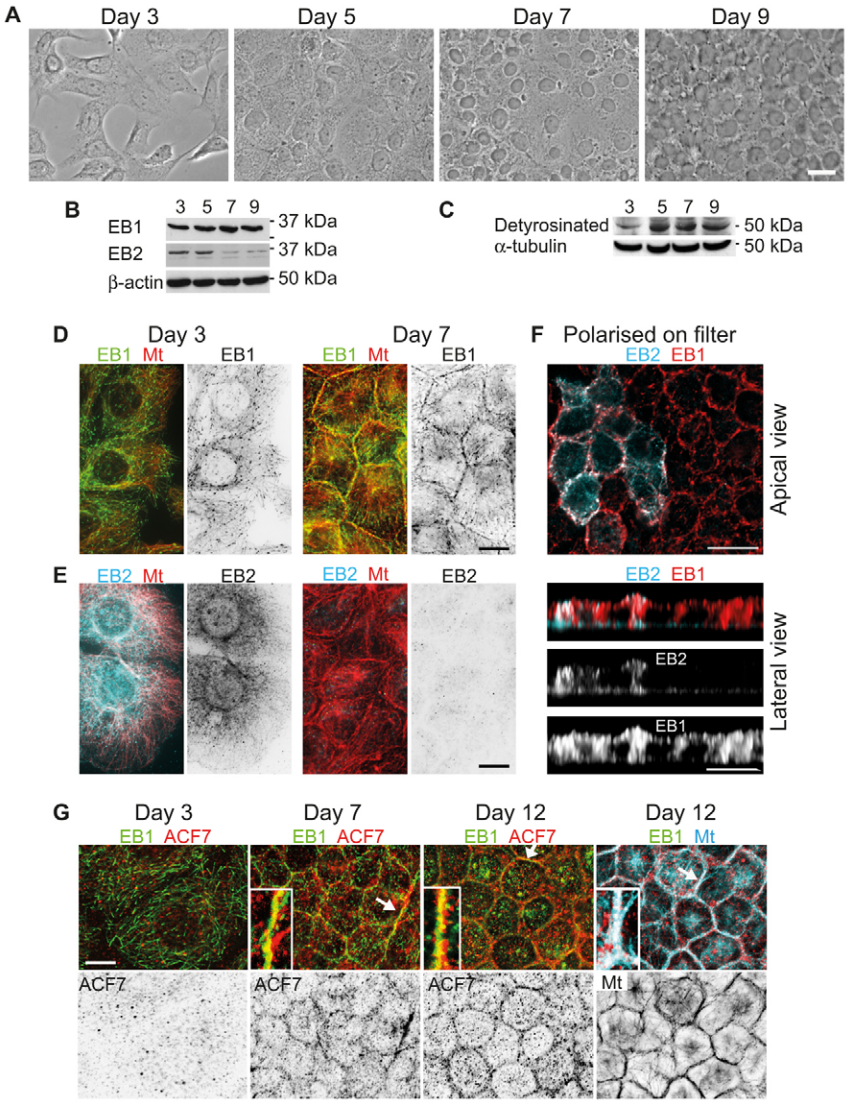

Fig. 1. EB2 is downregulated in most mIMCD-3 cells during apico-basal epithelial differentiation. (**A**) Phase-contrast images of cells at different stages of differentiation from subconfluent at day 3 to highly confluent (partially polarised) at day 9. (**B**,**C**) Western blots showing EB1, EB2 and β-actin protein levels at days 3, 5, 7 and 9 (B), and detyrosinated and total tubulin levels in (C). (**D**) Widefield fluorescence microscope images show distinct EB1 (rabbit pAb, green/invert) comets at microtubule (YL1/2, red) plus-ends at day 3 and peripheral accumulation at day 7. (**E**) Cells immunolabelled for α-tubulin (red) and EB2 (blue/invert) reveal relatively high expression of EB2 in subconfluent cells (day 3) but low expression in confluent cells (day 7). (**F**) Confocal optical sections of polarised cells grown on filter at day 7 showing a patch of high-expression EB2 (blue) cells surrounded by low-expression cells, whereas EB1 (rabbit pAb, red) expression is prominent in all. (**G**) Confocal sections of cells immunolabelled for ACF-7 (red) and either EB1 (mouse mAb, green) or tubulin (YL1/2, blue) showing dispersed ACF7 at day 3, but cortical ACF7 co-localising with EB1 and microtubules (arrows and enlargements in insets) at days 7 and 12. Scale bars: 20 µm (A); 10 µm (D–G). Mt, microtubule.

sheets (Fig. 1A). Western blots and immunolocalisation using highly specific antibodies (Komarova et al., 2005) showed that EB1 is stably expressed during epithelial differentiation while EB2 is downregulated (Fig. 1B,D,E). An increase in microtubule stability was indicated by an increase in detyrosinated tubulin as cells reached confluence (Fig. 1C). Although, EB1 protein levels remained the same during this differentiation period, EB1 localisation changed from microtubule plus-end in subconfluent cells (day 3) to mainly peripheral and apico-basal in confluent (day 7) and fully polarised cells (Fig. 1B,D,F). Interestingly, ACF7 localisation also changed from cytoplasmic and dispersed in subconfluent cells (day 3) to peripheral, co-localising with EB1 and microtubules in differentiated cells (days 7 and 12) (Fig. 1G). All subconfluent and early differentiating (days 3–5) cells showed relatively high EB2 expression, while the vast majority of confluent and fully polarised cells revealed very low expression of EB2 suggesting that downregulation of EB2 may be associated with epithelial differentiation (Fig. 1B,E,F). Interestingly, a few patches of confluent and polarised cells showed high levels of EB2 expression suggesting a heterogeneous population (Fig. 1F; supplementary material Fig. S1A). Confocal optical cross-sections and lateral views of Z stacks revealed that in EB2-expressing polarised cells EB2 showed a similar distribution to EB1 and co-localised with the apico-basal microtubules (Fig. 1F; supplementary material Fig. S1B). Both high and low EB2 expressing differentiated cells had elongated when grown on filters and appeared to assemble apico-basal microtubules. However, the precise organisation of the microtubules could not be defined due to lack of Z resolution.

siRNA depletion of EB2 induces formation of straight, bundled and less-dynamic microtubules

In order to determine whether EB2 downregulation affects microtubule organisation EB2 was depleted using siRNA in human retinal pigment epithelial cells (ARPE-19) as these contain a classic radial microtubule organisation and deviations from this pattern are easily detected (Bellett et al., 2009). ARPE-19 cells showed EB2 localisation in patches along microtubules and at plus-ends as previously reported for other cell lines (Fig. 2A) (Komarova et al., 2009). Four siRNA sequences (a–d) resulted in complete knockdown of EB2 at 96 hours after double transfection (0 and 48 hours) (Fig. 2B; supplementary material Fig. S1C). EB2 depletion produced a distinct phenotype with significantly larger cells containing straighter and often bundled microtubules compared to control (untreated) and scramble siRNA cells (Fig. 2C,D,E). Similar results were observed in U2OS, TC7 and HCT116 epithelial cells following EB2 knockdown (data not shown). EB2-depleted ARPE-19 cells were on average 3.7 times larger than scramble siRNA cells based on cell area (Fig. 2E). Cell proliferation assays and Ki-67 staining (Gerdes et al., 1984) revealed no significant differences between EB2-depleted and scramble siRNA cells within the 96 hour analyses period (supplementary material Fig. S2A,B,C). Live time-lapse imaging showed that even relatively large EB2-depleted cells were able to complete cell division (supplementary material Movies 1, 2).

Microtubule straightness was analysed by determining the number of microtubule crossover events within 10×10 μm squares. Significantly fewer crossover events were evident in EB2-depleted compared to control and scramble siRNA cells thus suggesting that EB2 depletion results in straighter microtubules (Fig. 2F). The possibility that the increase in straightness could be due to an increase in microtubule density was also assessed by determining the number of microtubules within the squares. However, no significant difference in microtubule numbers was observed between EB2 siRNA and scramble siRNA cells (supplementary material Fig. S2D). In order to verify these results a mCherry-tagged EB2 expression vector was generated using the mouse sequence, which is unaffected by the human siRNA sequences (supplementary material Fig. S2E,F). The mCherry–EB2 expressed in EB2-depleted cells associated with the microtubule lattice and successfully rescued both cell size and microtubule crossover event phenotypes (Fig. 2E,F,G). The average size of the rescued cells was significantly less than the EB2-depleted cells and the microtubules had more crossover events and were similarly organised to control/scramble siRNA cells (Fig. 2E,F).

Epithelial differentiation is known to be associated with an increase in microtubule stability (Pepperkok et al., 1990). In EB2-depleted ARPE-19 cells detyrosinated tubulin was particularly prominent in microtubule bundles (Fig. 3A). Increased microtubule stability was confirmed with cold treatment, with resistant microtubules evident in EB2-depleted, but not in control/scramble siRNA, cells (Fig. 3B, and data not shown). Furthermore, live time-lapse imaging of GFP–tubulin expressing ARPE-19 cells depleted for EB2 revealed a marked reduction in microtubule dynamics compared to control and scramble siRNA cells (Fig. 3C,D,E; supplementary material Movies 3, 4). Analyses (based on >60 microtubules per condition) revealed that EB2 depletion had no effect on microtubule growth but did cause a significant reduction in microtubule shrinking and an increase in pausing events (Fig. 3D). Graphic representation of microtubule profiles in terms of length changes over time showed minimal deviations, demonstrating reduced dynamics in EB2-depleted compared to scramble siRNA cells (Fig. 3E; supplementary material Fig. S2G). An increase in microtubule stability and bundle formation and a decrease in microtubule dynamics are evidently associated with EB2 depletion.

siRNA depletion of EB2 leads to EB1 association along the microtubule lattice

Epithelial differentiation in mIMCD-3 cells showed no change in the level of EB1 expression but a change in its distribution (Fig. 1). EB1 localisation was therefore investigated in ARPE-19 EB2-siRNA-treated cells. Both control and scramble siRNA cells showed the classic EB1 plus-end localisation (Fig. 4A). However, a marked change in EB1 deployment was observed in EB2-depleted cells with EB1 associating not only at the plus-ends but also along the length of the microtubule lattice (Fig. 4A). EB1 lattice association was also observed following EB2 depletion in U2OS, TC7 and HCT116 epithelial cells (data not shown). Predominant EB1 plus-end localisation could be rescued by expression of mCherry–EB2 in EB2-depleted cells (Fig. 4B). Both EB2 depletion and rescue phenotypes were verified by fluorescence intensity measurements. The fluorescence signal from random 2 μm segments along microtubules (but away from the plus-ends) revealed a significant increase in EB1 fluorescence intensity along the microtubule lattice in EB2-depleted compared to scramble siRNA cells while rescued cells showed a return to control fluorescence intensity levels (Fig. 4C).

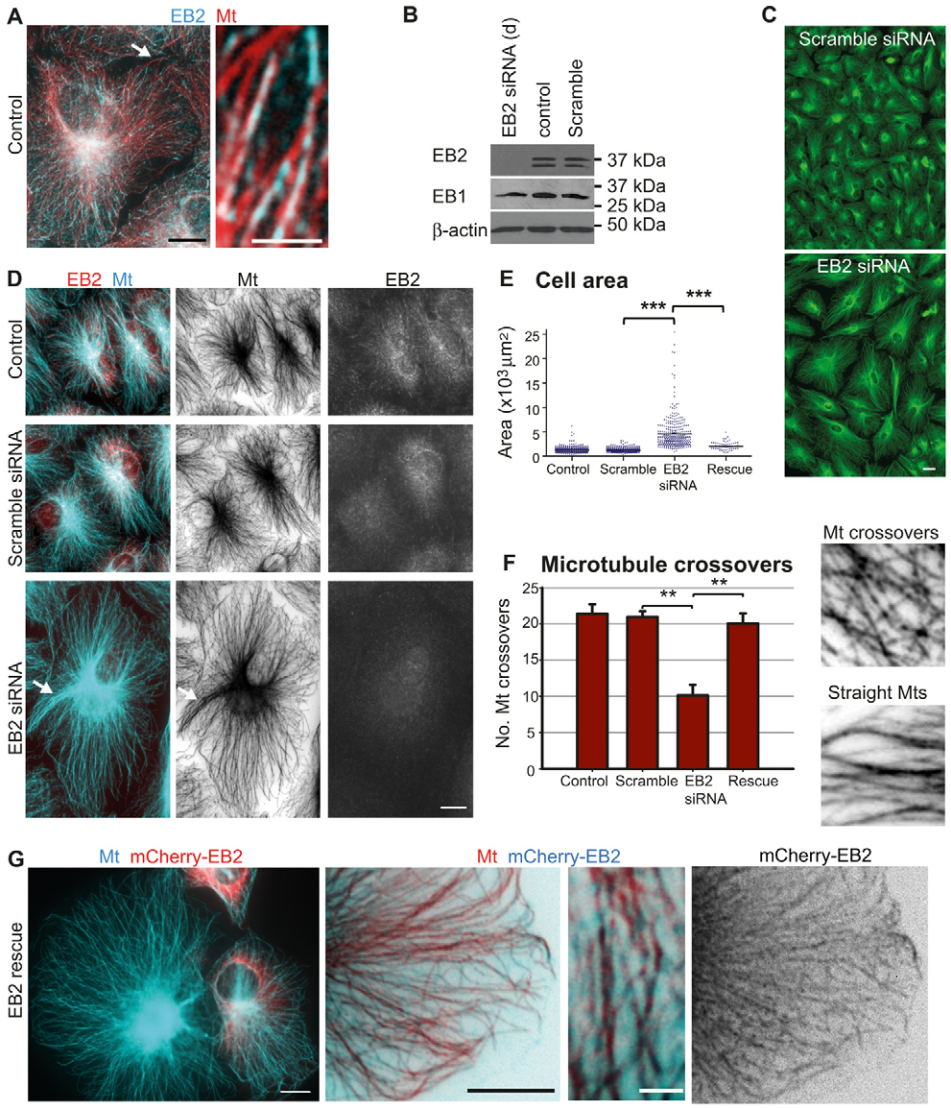

Fig. 2. siRNA depletion of EB2 in ARPE-19 cells leads to straight and bundled microtubules and increased cell size. (**A**) Widefield fluorescence images of an untreated control cell (enlarged region arrowed) showing EB2 (blue) at the plus-ends and along the microtubule (α-tubulin, red) lattice. (**B**) Western blots of cell lysates of control, scramble, EB2 siRNA (sequence d) at 96 hours post initial treatment showing EB2, EB1 and β-actin expression levels. (**C**) Image overviews highlight striking differences in cell size between scramble and EB2 siRNA-treated (sequence d) cells. Cells were fixed in paraformaldehyde to minimise cell shrinkage and were labelled for α-tubulin (green). (**D**) Widefield fluorescence images of control, scramble and EB2-siRNA-treated cells labelled for EB2 (red/single channel) and α-tubulin (blue/single channel) showing increased cell size, straight radial microtubules with some bundling (arrow). (**E**) Analysis of cell size based on cell area in control (n=311), scramble (n=311), EB2-siRNA-treated (sequence d, n=311) and mCherry–EB2 rescued (n=55) cells. (**F**) Average number of microtubule crossover events based on 15 peripheral squares (10×10 µm) in five cells, data averaged (±s.e.m.) from three independent experiments for each treatment. Images show typical examples of microtubule organisation in squares selected for analysis from control or scramble (microtubule crossovers) and EB2 siRNA-treated (straight microtubules) cells. (**G**) EB2-siRNA-depleted cell with straight and bundled microtubules (α-tubulin, blue) next to an mCherry–EB2-expressing (red) rescued cell showing curvy microtubules. Enlarged regions from an mCherry–EB2-expressing cell with mCherry–EB2 (blue, invert) associated along microtubules (red). See supplementary material Table S1 for summary of data and statistical testing. ***P<0.001, **P<0.01. Scale bars: 10 µm (A,D,G); 20 µm (C); 2 µm (A,G enlargements). Mt, microtubule.

We also found that Taxol induced microtubule stabilisation and bundle formation in ARPE-19 cells caused EB1 to become associated along microtubules as previously reported (Shannon et al., 2005). However, EB2 very rarely associated with the microtubule lattice in Taxol-induced bundles and remained cytoplasmic. EB3 did associate along microtubules, but to a lesser extent than EB1 (supplementary material Fig. S3A and data not shown). Furthermore, inactivation of the Rho effector ROCK with Y27632 in ARPE-19 cells, which is noted for inducing microtubule stability, resulted in microtubule bundling and formation of microtubule-rich cell protrusions as previously reported (Darenfed et al., 2007; Gao et al., 2004) but also led to a significant increase in EB1 lattice association compared to untreated controls (supplementary material Fig. S3B). This suggests that EB1 associates with the lattice of stable microtubules.

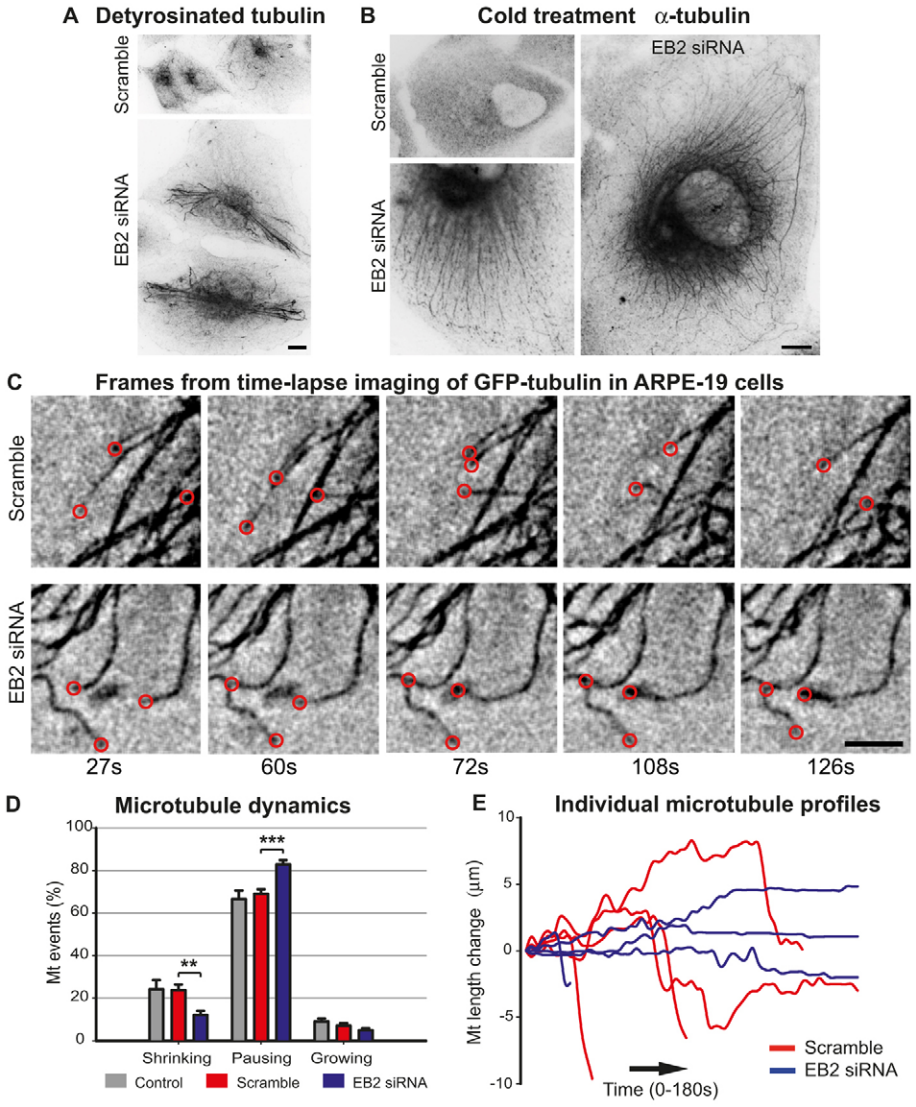

Fig. 3. EB2-siRNA-depleted ARPE-19 cells have more stable and less dynamic microtubules. (**A**) Scramble and EB2-siRNA-treated cells showing detyrosinated tubulin. (**B**) Cold-treated cells showing total loss of microtubules (α-tubulin) in scramble siRNA but resistant microtubules in EB2-depleted cells. (**C–E**) Control, scramble and EB2-siRNA-treated cells stably expressing GFP–α-tubulin imaged every 3 seconds for 3 minutes using a widefield fluorescence microscope. A total of 30 peripheral regions (12.5×12.5 μm) were analysed from $n=5$ control, scramble and EB2-depleted cells. (C) Image frames selected from a representative scramble and EB2-depleted region (see also supplementary material Movies 3,4). The microtubule plus-ends (red circles) show dynamic microtubules undergoing growth and shrinkage in the scramble siRNA cell, whereas the EB2-depleted cell shows less dynamic microtubules with many pausing events. (D) Analysis of average ($n=5$ cells ± s.e.m.) microtubule events scored every 3 seconds as either growing, shrinking or pausing in control (61 microtubules), scramble (61 microtubules) and EB2 siRNA (66 microtubules) cells. (E) Dynamic profiles of the microtubules selected in C from supplementary material Movies 3 and 4 for scramble and EB2-depleted cells, respectively. See supplementary material Table S1 for summary of data and statistical testing. ***$P<0.001$, **$P<0.01$. Scale bars: 10 μm (A,B), 5 μm (C). Mt, microtubule.

siRNA depletion of EB2 leads to ACF7 recruitment to microtubules and co-alignment with actin filaments

ACF7 has been reported to bind both microtubules and EB1, to cross-link microtubules and actin filaments, especially in the vicinity of cell junctions, and has been linked to increased microtubule stability (Karakesisoglou et al., 2000; Kodama et al., 2003; Wu et al., 2008). Our epithelial polarisation data showed a change in ACF7 distribution from dispersed at day 3 to cortical and co-localising with EB1 and microtubules at day 7 and 12 (Fig. 1) suggesting that EB1 binding along the microtubule lattice could recruit ACF7 and facilitate microtubule bundle formation. ACF7 localisation in control and scramble siRNA ARPE-19 cells was diffuse whereas distinct alignment along microtubules and some co-localisation with EB1 was observed in EB2-depleted cells (Fig. 5A). Again this phenotype could be rescued with mCherry–EB2 (Fig. 5B). The significant shift in ACF7 distribution from dispersed in control/scramble siRNA cells to alignment along microtubules in EB2-depleted cells and the subsequent rescue by mCherry–EB2 expression was confirmed by fluorescence intensity analyses (Fig. 5C). We were unable to determine whether this change in ACF7 localisation was associated with an increase in ACF7 expression or merely a redistribution of the existing pool. EB1 binding along the microtubule lattice and ACF7 association with microtubules, either directly or via EB1, could thus facilitate microtubule-actin filament co-alignment, cross linkage and bundle formation. Indeed, actin reorganisation was apparent with control/scramble siRNA cells showing mainly cortical actin and stress fibres while EB2-depleted cells revealed a reduction in stress fibres and increase in actin filaments and bundles oriented perpendicular to the cortex (Fig. 5D). Furthermore, using both confocal and electron microscopy microtubule-actin filament co-alignment was evident in EB2-depleted cells with microtubule bundles interdigitating with bundles of actin filaments (Fig. 5D,E). In the electron microscope single microtubules could also be seen aligned parallel to actin filaments and actin filaments were evident within microtubule bundles (Fig. 5E).

However, in Taxol induced bundles in ARPE-19 cells, which do not contain interdigitating actin filaments, ACF7 remained cytoplasmic and did not appear to align along microtubules as EB1 did (supplementary material Fig. S3A). Similarly, ROCK inhibition with Y27632 did not result in ACF7 recruitment to the

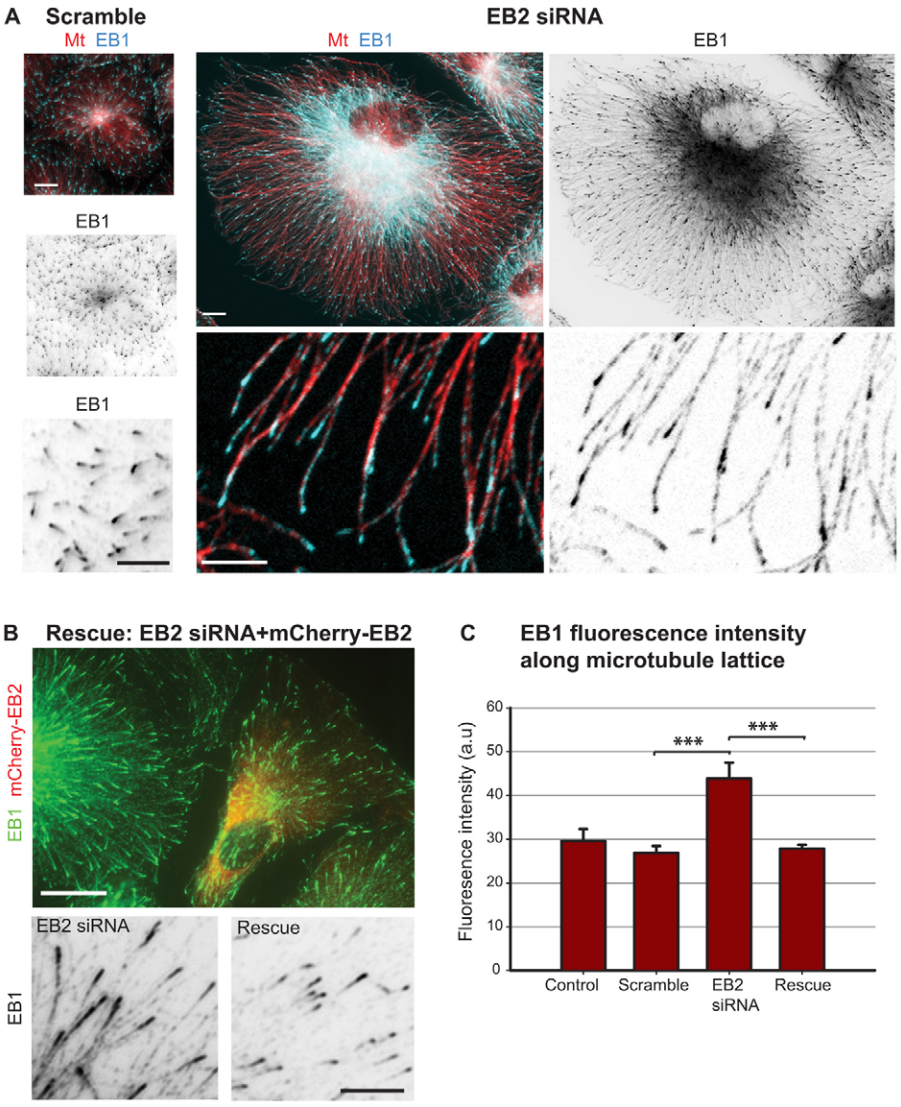

Fig. 4. EB1 associates with the microtubule lattice in EB2-siRNA-depleted ARPE-19 cells. (**A**) Scramble and EB2-siRNA-treated cells labelled for EB1 (mouse mAb, blue/inverts) and α-tubulin (red). Enlarged peripheral region of scramble cell shows distinct EB1 (invert) comets with little or no tail. Enlarged region of EB2-depleted cell shows EB1 (blue, invert) at plus-end and along the microtubule (red) lattice. (**B**) EB2-siRNA-depleted cells transiently transfected with mCherry–EB2 (red) 24 hours before fixation and labelled for EB1 (mouse mAb, green/invert) showing an mCherry–EB2 rescued cell next to a depleted cell. Invert images show EB1 localisation along microtubules in the depleted cell and plus-end comet restoration in the rescued cell. (**C**) Data analysis showing average (n=25 microtubules ±s.e.m.) EB1 fluorescence intensity in control, scramble, EB2-siRNA-treated and rescued cells. See supplementary material Table S1 for summary of data and statistical testing. ***P<0.001. Scale bars: 10 µm (A,B); 5 µm (enlargements). Mt, microtubule.

microtubule lattice nor did it lead to preferential co-alignment of microtubules and radial actin filaments, except within cell projections that also contained actin filaments (supplementary material Fig. S3B,C,D and data not shown). This suggests that microtubule stability and EB1 lattice association is not sufficient to recruit ACF7 and facilitate microtubule-actin filament co-alignment. Furthermore, it seems that ACF7 recruitment to microtubules requires actin filaments.

Double depletion of EB2 and EB1 does not rescue the control phenotype but reveals EB3 compensation

The importance of lattice associated EB1 in terms of microtubule organisation and ACF7 recruitment and co-alignment with actin filaments was further investigated in ARPE-19 cells by double depletion of EB2 and EB1. Double depletion would be expected to rescue the control phenotype if EB1 lattice association is central to the EB2 depletion phenotype.

Simultaneous double transfection (0 and 48 hours) with siRNAs for EB2 and EB1 resulted in knockdown of both proteins (Fig. 6A). No discernable differences in microtubule straightness or organisation were evident in double-depleted cells compared to EB2 only depleted cells (compare Fig. 6A,C,E and Fig. 2D; Fig. 4A and Fig. 5A). Microtubule bundles were evident in EB2/EB1 double-depleted cells as also found in EB2-depleted cells (Fig. 6A,E). The microtubules appeared straighter in EB2/EB1 double-depleted cells compared to scramble siRNA cells as confirmed by microtubule crossover event analysis which revealed significantly fewer crossover events in double-depleted compared to scramble siRNA cells (Fig. 6B).

Interestingly, EB3 associated along the length of the microtubules as well as at the plus-ends in cells double depleted for EB2 and EB1 (Fig. 6C). This is unlike control, scramble and EB2-siRNA-treated ARPE-19 cells, which showed dispersed cytoplasmic distribution of EB3 (Fig. 6C and data not shown). Increased EB3 microtubule lattice association in EB2/EB1 double-depleted cells was verified by fluorescence intensity measurements (Fig. 6D). Furthermore, an increase in ACF7 association along the length of microtubules was evident in double-depleted cells as found for EB2-depleted cells and this was verified by fluorescence intensity analyses (Fig. 6E,F).

This suggests that EB3 can compensate for EB1, associate along the microtubule lattice and maintain the EB2-depleted phenotype.

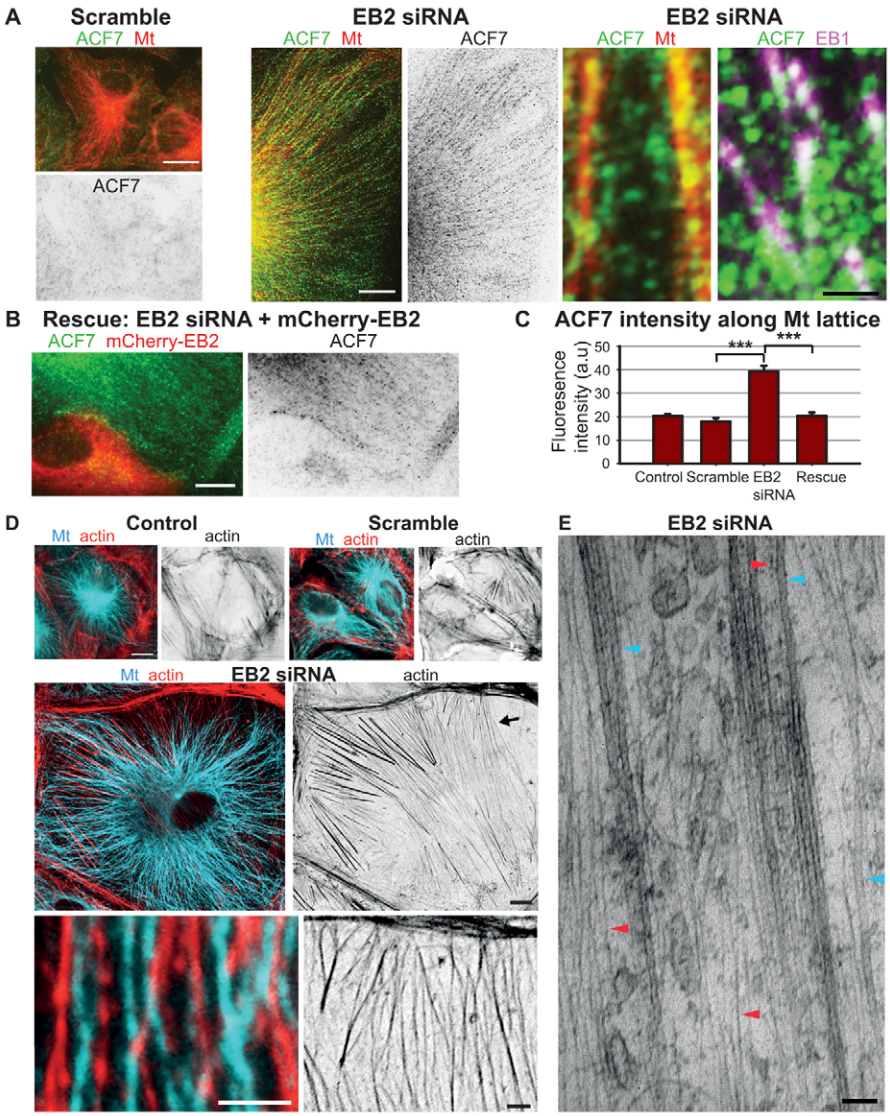

Fig. 5. EB2 depletion in ARPE-19 cells leads to ACF7 localisation along microtubules and co-localisation with EB1 and microtubule-actin filament co-alignment. (**A**) Scramble and EB2-siRNA-treated cells labelled for ACF7 (green/invert) and tubulin (YL1/2, red). ACF7 is dispersed in scramble siRNA cells but is associated along the microtubule lattice and co-localises with EB1 (mouse mAb, purple) in EB2-depleted cells (highlighted in enlarged images). (**B**) EB2-siRNA-depleted cells transiently transfected with mCherry–EB2 (red) 24 hours before fixation showing loss of ACF7 (green/invert) microtubule association in the rescued cell. (**C**) Data analysis showing average (n=25 microtubules ± s.e.m.) ACF7 fluorescence intensity in control, scramble siRNA, EB2-siRNA-treated and rescued cells. (**D**) Control, scramble and EB2-siRNA-treated cells stained for actin (phalloidin, red/invert) and α-tubulin (blue) showing mainly peripheral actin and stress fibres, and little alignment with microtubules in control and scramble siRNA cells, whereas microtubule–actin filament co-alignment is prominent in depleted cells. Enlarged regions of EB2-depleted cells show radial actin filaments oriented perpendicular to the cortex and microtubule-actin filament co-alignment and interdigitation. (**E**) Transmission electron micrograph from EB2-siRNA-depleted cell showing microtubule (blue arrowheads) and actin filament (red arrowheads) bundles co-aligned, as well as single actin filaments within microtubule bundles. See supplementary material Table S1 for summary of data and statistical testing. ***P<0.001. Scale bars: 10 μm (A,B,D); 2.5 μm (enlargements); 50 nm (E).

Unfortunately, triple depletion of EBs is lethal and could thus not be used to determine the role of EB1/EB3 in microtubule straightness and bundle formation (Komarova et al., 2009).

siRNA depletion of EB2 but not EB1 prevents initial microtubule reorganisation during apico-basal epithelial differentiation, whereas depletion of either inhibits microtubule bundle formation and epithelial elongation

Our findings show that low EB2 expression promotes microtubule stability, EB1 lattice binding and bundle formation. Therefore EB2 expression may be required to ensure a dynamic microtubule population to enable reorganisation. To further investigate the role of EB2 and EB1 in microtubule reorganisation and apico-basal bundle formation EB2 and EB1 were depleted separately in differentiating human colonic epithelial (TC7) cells as they readily polarise producing 10–12 μm tall cells when grown to confluence.

EB1 or EB2 siRNA triple treatments (0, 48 and 96 hours) of TC7 cells resulted in knockdown of both proteins (Fig. 7A). Lateral views of three-dimensional reconstructions of optical confocal sections revealed a lack of apico-basal elongation in both EB1- and EB2-depleted cells (Fig. 7B). Single optical cross-sections through apical, medial and basal regions of scramble siRNA cells showed typical polarised epithelial microtubule organisation with apical and basal networks and apico-basal bundles as evidenced by peripheral rings in medial cross-sections (Fig. 7C). This was lost in EB2-depleted cells. Instead, the microtubule networks were typical of undifferentiated epithelial cells (Fig. 7C). Unlike EB2 knockdown, optical cross-sections of EB1-depleted cells showed similar apical and basal microtubule organisation to that of scramble siRNA cells and some peripheral microtubules in medial sections. However, the peripheral bundles were not oriented apico-basally (Fig. 7C). Furthermore, both EB1 and EB2 depletion caused significant decrease in cell height and increase in area compared to scramble treatment (Fig. 7B,C,D). However, while EB1 depletion caused some cell constriction this was not the case for EB2 depletion, which resulted in cells with large surface areas typical of subconfluent cells (Fig. 7C,D).

These findings suggest that EB2 but not EB1 expression is critical for initial microtubule reorganisation and cell constriction whereas EB1 is important for apico-basal microtubule bundle

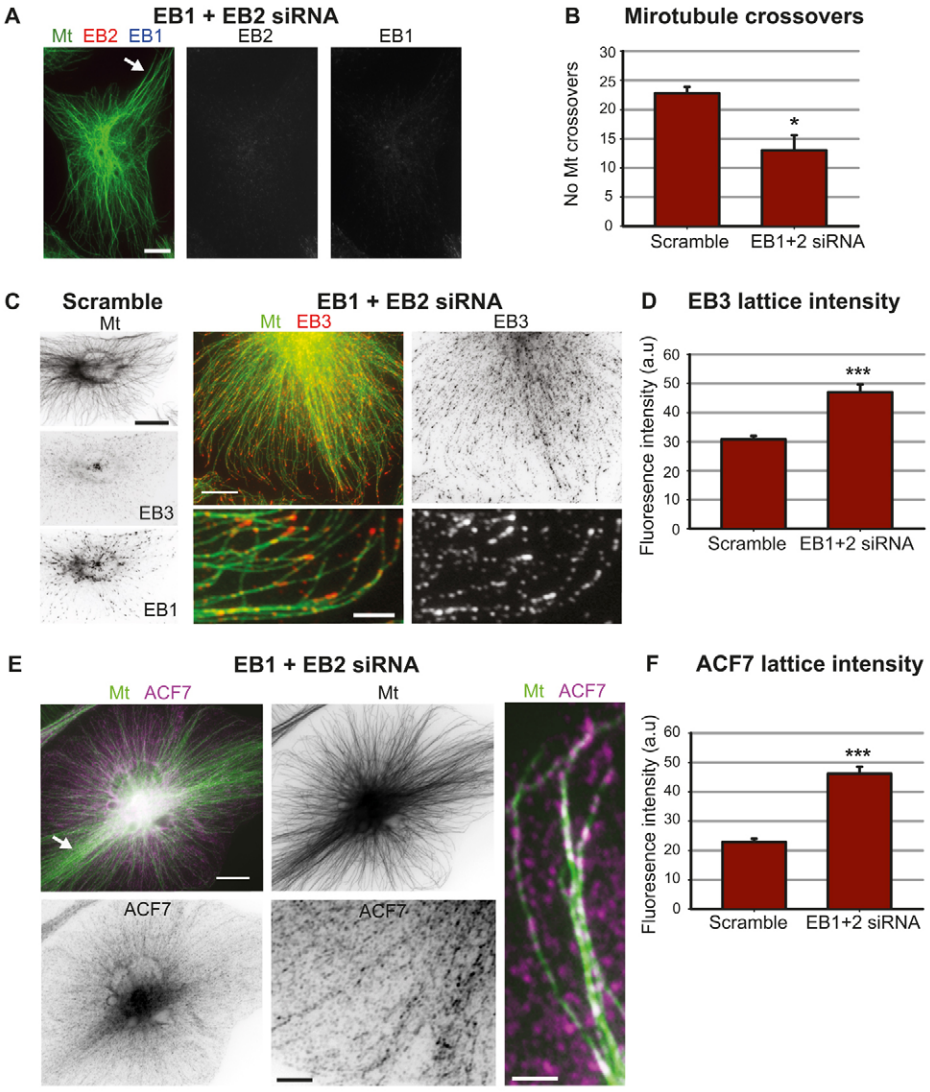

Fig. 6. Double depletion of EB2 and EB1 in APRE-19 cells does not rescue the control phenotype but reveals EB3 compensation. (**A**) Widefield fluorescence images (exposure levels set to scramble cells not shown) showing a cell treated with both EB1 and EB2 siRNA, labelled for α-tubulin (green), EB2 (red channel) and EB1 (mouse mAb blue channel), showing knockdown of both proteins and microtubule bundling (arrow). (**B**) Average number of microtubule crossover events based on 15 peripheral squares (10×10 µm) in five cells with data averaged (± s.e.m.) from three independent experiments for each treatment. (**C**) Inverted images of microtubules (α-tubulin), EB3 (KT36) and EB1 (mAb) in a scramble siRNA cell. EB1- and EB2-siRNA-depleted cell showing α-tubulin (green) and EB3 (KT36, red, invert). Enlarged region showing EB3 (red, single channel) localisation to microtubule plus-ends and along the lattice. (**D**) Data analysis showing average (n=25 microtubules ± s.e.m.) EB3 fluorescence intensity along microtubule lattice in scramble and EB1- and EB2-siRNA-treated cells. (**E**) EB1- and EB2-depleted cell showing α-tubulin (green, invert) and ACF7 (purple/invert). Enlarged regions highlights ACF7 localisation along the microtubule lattice. (**F**) Data analysis showing average (n=25 microtubules ± s.e.m.) ACF7 fluorescence intensity along the microtubule lattice in scramble and EB1- and EB2-siRNA-treated cells. See supplementary material Table S1 for summary of data and statistical testing. *P<0.05, ***P<0.001. Scale bars: 10 µm (A,C,E); 2.5 µm (enlargements).

formation and epithelial elongation. Furthermore, the results suggest that while EB3 may be able to compensate for lack of EB1 during early stages of microtubule reorganisation it can not for apico-basal bundle formation.

Formin inhibition in EB2-depleted cells rescues the control phenotype

Increased microtubule stability, actin filament reorganisation and co-alignment of microtubules and actin filaments following EB2 knockdown or downregulation suggest involvement of the Rho GTPases and their downstream effectors, the formins. The perpendicular actin bundles evident in the EB2-depleted cells (Fig. 5D) resemble dorsal/radial filaments associated with lamellipodia that are activated by Rac1 and assembled by mDia formins. In addition, expression of the FH1/FH2 domains of several formins have been shown to induce microtubule stability as well as co-alignment with actin filaments (Bartolini and Gundersen, 2010; Gasteier et al., 2005; Ishizaki et al., 2001; Kobielak et al., 2004; Kovac et al., 2013; Oakes et al., 2012; Ryu et al., 2009; Thurston et al., 2012; Yang et al., 2007). The role of formins in microtubule straightness, co-alignment with actin filaments and EB1 and ACF7 lattice association in EB2-depleted cells was therefore investigated. EB2-depleted cells were treated with the formin inhibitor SMIFH2 (Rizvi et al., 2009), which specifically inhibits the FH2 domain and affects both actin filament assembly and formin interactions with microtubules.

Formin inhibition with 10 µM SMIFH2 for 40 minutes in EB2-depleted ARPE-19 cells resulted in less-organised microtubules that lacked co-alignment with actin filaments and showed predominant EB1 plus-end and cytoplasmic ACF7 localisation (Fig. 8). SMIFH2 caused a reduction in radial actin filaments oriented perpendicular to the cortex and an increase in stress fibres (Fig. 8A). The microtubules often curled at the periphery and analysis of crossover events revealed a significant increase in SMIFH2-treated EB2-depleted compared to EB2-depleted (+DMSO) cells, but not compared to scramble siRNA (+DMSO) cells (Fig. 8A,C). Predominant EB1 plus-end localisation was restored with EB1 lattice fluorescence intensities showing a significant decrease in SMIFH2-treated EB2-depleted compared to EB2-depleted (+DMSO) cells while not compared to scramble siRNA (+DMSO) cells (Fig. 8B,D). Furthermore, a significant reduction in ACF7 fluorescence

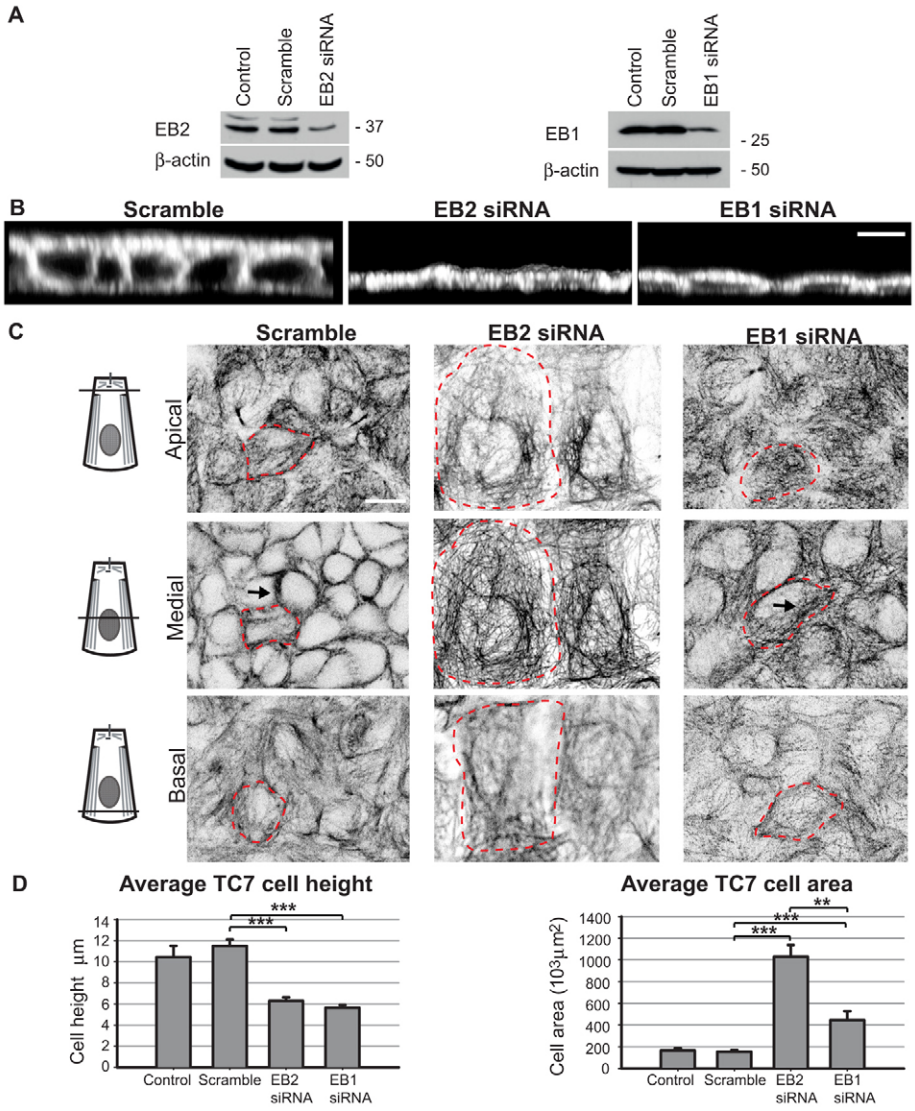

Fig. 7. EB2 depletion in TC7 cells prevents microtubule reorganisation and apico-basal elongation, whereas EB1 depletion affects elongation but not reorganisation. (**A**) Western blots of extracts taken at 144 hours from control, scramble, EB2- and EB1-siRNA-treated (0 hours, 48 hours, 96 hours) cells, showing EB2, EB1 (mouse mAb) and β-actin expression. (**B**) Lateral views of 3D reconstructions of scramble, EB2- and EB1-siRNA-treated cells (to scale) labelled for α-tubulin showing a reduction in cell height in EB2-depleted and EB1-depleted cells. (**C**) Confocal optical cross-sections through apical, medial and basal regions (see diagrams, line represents level of section) of representative scramble, EB2 and EB1 siRNA cells stained for α-tubulin. One cell from each condition is highlighted (red dotted line) in each section. All sections show large cell areas and lack of cellular constriction in EB2-depleted cells compared with scramble siRNA and EB1-depleted cells. Medial sections show distinct peripheral microtubule rings (arrow) representing cross-sections of the apico-basal microtubules in scramble cells; there is a total lack of these in EB2-depleted cells and mis-oriented bundles (arrow) in EB1-depleted cells. (**D**) Analysis of epithelial differentiation in terms of cell height and area in 143 µm×143 µm boxed regions in control (height, area $n=3$), scramble (height $n=8$, area $n=6$), EB1-siRNA-treated (height, area $n=4$) and EB2-siRNA-treated (height $n=9$, area $n=6$) cells. Data pooled from three separate experiments. See supplementary material Table S1 for summary of data and statistical testing. $^{**}P<0.01$, $^{***}P<0.001$. Scale bar: 10 µm.

intensity along microtubules was evident in SMIFH2-treated EB2-depleted compared to EB2-depleted (+DMSO) cells while not compared to scramble siRNA (+DMSO) cells (Fig. 8B,E). Formin inhibition of EB2-depleted cells thus seemed to rescue the control/scramble siRNA phenotype by increasing microtubule crossover events, decreasing co-alignment with actin filaments and restoring predominant EB1 plus-end and cytoplasmic ACF7 localisation.

The data suggest that formin activation is involved in creating the EB2-depleted phenotype in epithelial cells.

Inner ear and intestinal epithelia reveal a direct correlation between low EB2 expression and the presence of distinct apico-basal microtubule bundles

The *in vitro* cultured epithelial cell data suggest that EB2 downregulation or knockdown promotes microtubule bundle formation, EB1 lattice binding, ACF7 recruitment and co-alignment with actin filaments. However, it is important to determine *in vivo* whether there is a correlation between low level EB2 expression and the presence of distinct apico-basal microtubule bundles in polarised epithelial cells. The organ of Corti in the inner ear contains highly organised rows of sensory hair (mechanoreceptors) and supporting cells (transmit sound induced vibrations to the hair cells) (Fig. 9A). Both cell types are apico-basally polarised and terminally differentiated but only the supporting cells contain stable apico-basal microtubule bundles with interdigitating actin filaments (Fig. 9Ai,ii,vii,viii). By contrast, the majority of the microtubules in the hair cells are dynamic and free in the cytoplasm (Fig. 9Ai, iii) (Bane et al., 2002; Furness et al., 1990; Mogensen et al., 2002; Slepecky et al., 1995; Tucker et al., 1992). A distinct pattern of EB2 expression was evident in the organ of Corti with high expression of EB2 in all hair cells but very low level of expression in the supporting cells (Fig. 9Aiv,v). EB1 was also found to associate along the microtubule bundles in the supporting cells (Fig. 9Avi).

Unlike the inner ear cells the epithelium of the intestinal crypt is not terminally differentiated but undergoes rapid turnover and contains both proliferating and differentiating epithelial cells. Stem cells located at the base of the crypt give rise to transit-amplifying cells that divide, differentiate and migrate up the crypt (van der Flier and Clevers, 2009). Immunolabelling for EB2 again showed a distinct pattern with high levels of EB2 expression in cells located within the basal stem cell region while

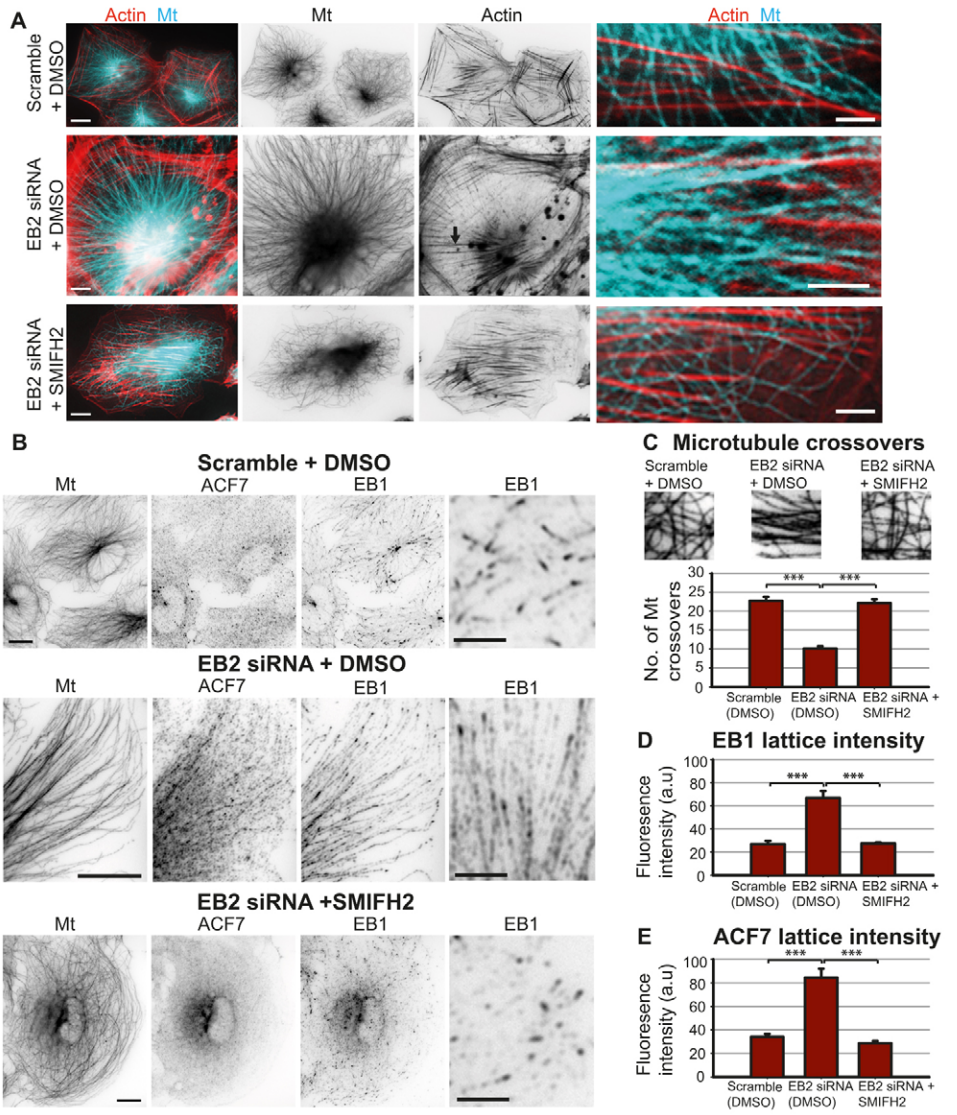

Fig. 8. Formin inhibition in EB2-depleted cells rescues the control phenotype. (**A**) Scramble (+DMSO), EB2-depleted (+DMSO) and formin-inhibited (10 μM SMIFH2 for 40 minutes) EB2-depleted ARPE-19 cells stained for α-tubulin (blue, invert) and actin (phalloidin, red, invert). Lack of straight microtubules and radial actin filaments oriented perpendicular to the cortex (arrow) are evident in SMIFH2-treated EB2-depleted cells. Enlarged regions highlight reversion to the scramble phenotype in SMIFH2-treated EB2-siRNA-depleted cells with a lack of microtubule–actin filament co-alignment. (**B**) Scramble (+DMSO), EB2-depleted (+DMSO) and formin-inhibited (10 μM SMIFH2 for 40 minutes) EB2-depleted ARPE-19 cells labelled for microtubules (YL1/2 invert), ACF7 (invert) and EB1 (mouse mAb, invert). Formin-inhibited EB2-depleted cells show extensive microtubule curving, dispersed ACF7 and a lack of EB1 microtubule lattice association similar to scramble cells (see enlarged regions of EB1 staining). (**C**) Average (n=3, ±s.e.m.) number of microtubule crossover events based on 15 peripheral squares (10×10 μm) in five cells from three independent experiments for scramble (+DMSO) treated, EB2-siRNA (+DMSO)-depleted and formin-inhibited EB2-siRNA (10 μM SMIFH2 for 40 minutes) cells. (**D**,**E**) Average (n=25 microtubules ±s.e.m.) microtubule lattice fluorescence intensities of EB1 (D) and ACF7 (E) in scramble (+DMSO), EB2 siRNA (+DMSO) and formin-inhibited EB2-siRNA-depleted cells. See supplementary material Table S1 for summary of data and statistical testing. ***P<0.001. Scale bars: 10 μm (A,B); 5 μm (enlargements).

low expression was evident in the cells above this region (Fig. 9Bi,iii). Interestingly, the apico-basal microtubules in cells within the basal region were curly and did not form distinct bundles (Fig. 9Biv). Instead, they displayed an umbrella-like organisation with microtubules focused on an apical centrosome (Fig. 10Ai). However, distinct apico-basal microtubule bundles were evident in the cells above this region where EB2 expression was low (Fig. 9Bi,ii; Fig. 10Aii). Both EB1 and ACF7 localised along the apico-basal microtubule bundles in the transit-amplifying and differentiated cells while EB1 was evident mainly along the baso-lateral and basal sides in cells within the basal region (Fig. 9Bii,iv; supplementary material Fig. S4).

A correlation between EB2 downregulation and the presence of distinct apico-basal microtubules is thus apparent in both terminally differentiated (inner ear) and proliferating (intestinal crypt) polarised epithelial tissue. The *in situ* data also indicated that EB2 expression is prominent in cells with dynamic microtubules.

Discussion

Dynamic behaviour of microtubules is essential for their reorganisation during apico-basal epithelial differentiation. Our findings suggest that EB2 expression during early stages of differentiation helps to maintain microtubule dynamics. EB2 downregulation leads to increased microtubule stability, the association of EB1 along the lattice and bundle formation, as well as ACF7 recruitment and co-alignment of microtubules and actin filaments. Similar results were obtained from both *in vitro* epithelial differentiation and *in situ* epithelial tissue analyses. siRNA depletion, rescue and microtubule dynamics studies further confirmed the central role of EB2 in epithelial differentiation.

Analyses of epithelial differentiation revealed that EB2 is expressed during early stages of differentiation when cell–cell contacts, apical constriction and major microtubule reorganisation occur whereas it is downregulated in most confluent and polarised epithelial cells. EB2 depletion during early stages of differentiation inhibited microtubule reorganisation, apical cell constriction and thus also apico-basal elongation. Lack of microtubule reorganisation is most likely due to less dynamic microtubules. This is supported by our data from cold induced depolymerisation and live cell imaging of GFP–tubulin-expressing ARPE-19 cells where EB2 depletion resulted

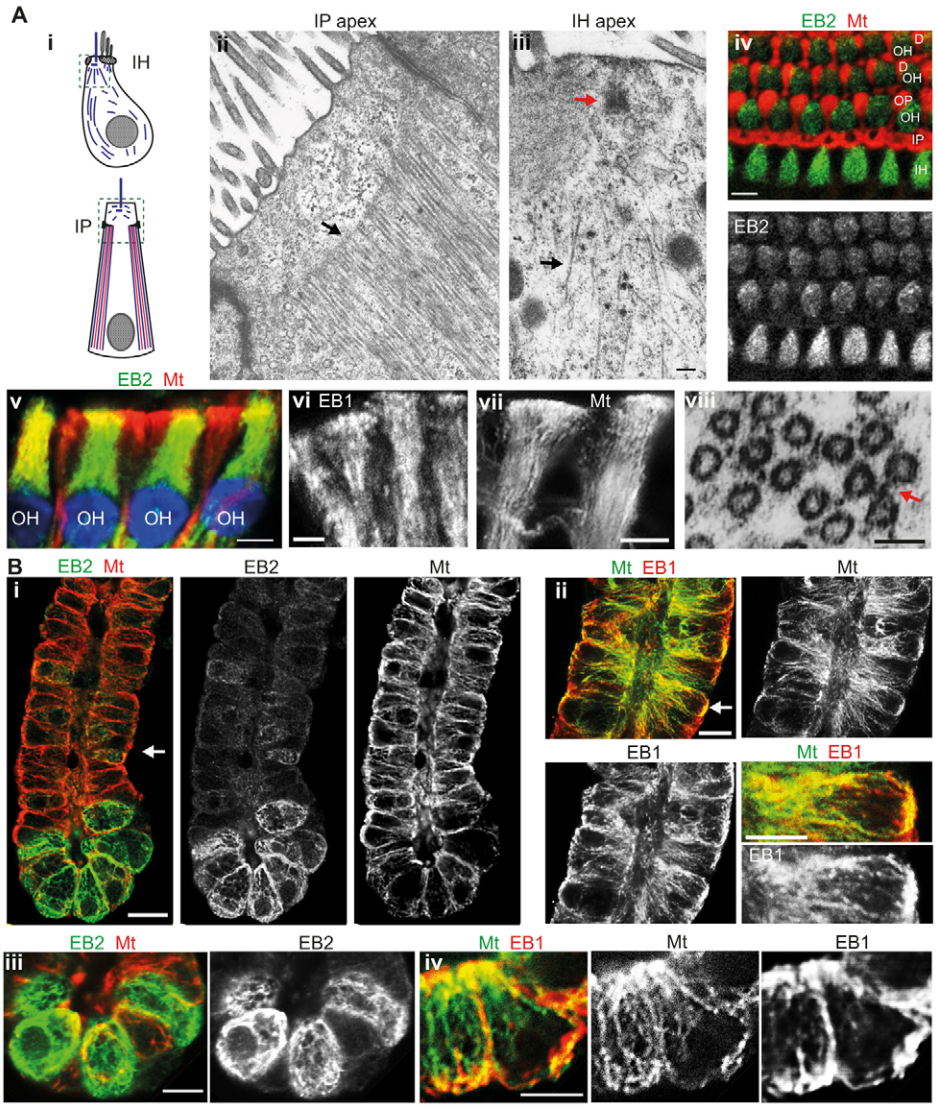

Fig. 9. Isolated inner ear (organ of Corti) and intestinal (crypt) epithelia reveal a correlation between low EB2 expression and the presence of distinct apico-basal microtubule bundles. (**A**) Isolated P4 mouse Organ of Corti. (i) Schematic diagrams of inner hair (IH) and inner pillar (IP) cells with microtubules in blue, actin filaments in red and non-centrosomal anchoring sites in black. The IH cell contains mainly free cytoplasmic microtubules (based on Furness et al., 1990), whereas the IP cell contains an apico-basal bundle of microtubules with interdigitating actin filaments, anchored at non-centrosomal sites. Boxed regions indicate the areas covered in TEM images (ii,iii). (ii) Electron micrograph of the apical region in an inner pillar cell showing part of the apico-basal bundle of microtubules anchored at non-centrosomal sites (arrow). (iii) Electron micrograph of the apical centrosomal/basal body (red arrow) region of an inner hair cell showing a fascicle (black arrow) of microtubules and lack of bundling. (iv) Apical view of Organ of Corti with rows of inner hair (IH), outer hair (OH) and supporting cells [inner pillar (IP), outer pillar (OP) and Deiters (D)] showing high EB2 (green/single channel) expression in IH and OH cells, whereas the expression of EB2 is low in all supporting cells (α-tubulin, red). (v) Lateral view showing OH and supporting cells with EB2 (green) co-localising with microtubules (red) in the OH cells, whereas supporting cells are low in EB2 expression. (vi) Lateral view of apical region of pillar cells showing EB1 (rabbit pAb) along the apico-basal microtubules. (vii) Lateral view of apical region of pillar cells showing apico-basal microtubule (α-tubulin) bundles. (viii) TEM image showing part of a cross-section through a pillar cell with actin filaments between microtubule and cross-links evident (red arrow). (**B**) Isolated adult mouse small intestinal crypts. (Bi) Lateral view of crypt labelled for α-tubulin (red, single channel) and EB2 (green, single channel) showing high EB2 expression in basal cells. (ii) Transit-amplifying region (arrow in i) showing low EB2 expression with EB1 (red, single channel) along apico-basal microtubules (YL1/2, green, single channel). Enlarged region (arrow) highlights EB1 localisation along apico-basal microtubule bundles. (iii) Basal crypt epithelial cells expressing EB2 (green, single channel) showing EB2 along curvy microtubules (YL1/2, red), (iv) Basal crypt epithelial cells showing curvy microtubules (YL1/2 green, single channel), lack of straight bundles and umbrella-like organisation with EB1 (red, single channel) mainly restricted to cortical areas. Scale bars: 100 nm (Aii,iii); 5 μm (Aiv–vii; B); 50 nm (Aviii).

in more stable and less dynamic microtubules. Decreased microtubule dynamics may also lead to mis-localisation and inactivation of Rho/ROCK/myosinII signalling required for apical actomyosin cortical contraction thus resulting in less cell constriction as observed in EB2-depleted cells (Siegrist and Doe, 2007).

Analyses of *in situ* inner ear and intestinal crypt epithelial tissue revealed a striking correlation between low EB2 expression

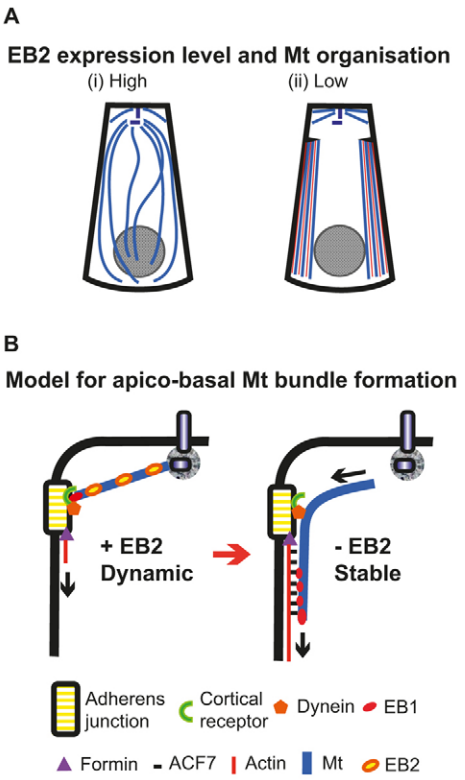

Fig. 10. Models for EB2 expression and apico-basal microtubule bundle formation. (A) EB2 expression level and apico-basal microtubule organisation. Schematic diagrams of microtubule organisation on the basis of EB2 expression levels. (i) High-EB2-expressing cell with unbundled curvy microtubules (blue) organised in an umbrella-like fashion (ii) Low-EB2-expressing cell with distinct apico-basal microtubule (blue) bundles co-aligned with actin filaments (red). **(B)** Model for apico-basal microtubule bundle formation. EB2 expression (+EB2) maintains a dynamic microtubule population during the early stages of differentiation. The centrosome nucleated microtubule elongates towards the cell periphery with EB2 associated along the lattice. The microtubule plus-end is captured at the adherens junction, a process mediated by +TIPs and cortical receptors (Bellett et al., 2009). Activation of junction-associated formin initiates actin cable assembly and elongation. The downregulation of EB2 (−EB2) at latter stages of differentiation facilitates bundle formation. Cortical-anchored dynein mediates microtubule release from the centrosome, and actin cables guide microtubules downwards facilitated by EB1 and ACF7. EB1 lattice binding and ACF7 cross-linkage lead to microtubule–actin filament co-alignment and the formation of a stable apico-basal bundle. Mt, microtubule.

and the presence of distinct apico-basal microtubule bundles that co-aligned with actin filaments and high EB2 expression and lack of such bundles. Interestingly, high expression of EB2 in polarised epithelial cells did not prevent apico-basal microtubules from forming but it did prevent them from organising into distinct straight bundles. This is supported by recent data on FGF (Fibroblast Growth Factor) signalling in cochlear development where loss of function of FGF-Receptor3 has been linked to EB2 (MAPRE2) gene upregulation and reduced microtubule bundle formation in cochlear pillar cells (Szarama et al., 2012).

The expression level of EB1 remained constant during epithelial differentiation. However, a distinct shift from a mainly plus-end to microtubule lattice association was evident and this coincided with an increase in microtubule stability. This was particularly evident following EB2 siRNA depletion. EB1 lattice association has been reported in differentiated myotubes and Sertoli cells and EB1 lattice binding has been suggested to enforce lateral protofilament interactions and thus increase microtubule stability (des Georges et al., 2008; Sandblad et al., 2006; Vitre et al., 2008; Wang et al., 2008; Wen et al., 2004; Zhang et al., 2009). EB1 lattice association was also observed along Taxol and Y27632 stabilised microtubules suggesting that stabilisation may facilitate EB1 lattice binding and this may in turn lead to further stabilisation. Interestingly, GTP–tubulin patches have been identified within the microtubule lattice and with EB1s affinity for this stable form an increase in GTP–tubulin could facilitate EB1 lattice binding (Dimitrov et al., 2008). This is supported by studies on axonal microtubules that have shown co-localisation of GFP–EB1 with patches of GTP–tubulin along the lattice (Nakata et al., 2011).

EB2 depletion also resulted in ACF7 association along the microtubules and differentiated epithelial crypt cells showed ACF7 along the apico-basal bundles. ACF7 and the *Drosophila* homologue Shot have previously been reported to bind along microtubules, acting as a MAP to stabilise microtubules. Most interestingly, ACF7 and EB1 have been suggested to guide microtubules along actin filaments with ACF7 depletion leading to unbundled and disorganised microtubules (Alves-Silva et al., 2012; Kodama et al., 2003; Wu et al., 2008). However, EB1 association along the microtubule lattice is not sufficient to recruit ACF7 as Taxol and Y27632 stabilised microtubules did not contain ACF7 along their length. Only cell projections that contained microtubules and actin filaments showed ACF7 localisation suggesting that actin filaments influence ACF7 deployment. It is also possible that the observed redeployment of ACF7 is linked to an upregulation in ACF7 triggered by EB2 depletion or downregulation but future investigations are needed to resolve this.

Cross-talk between microtubules and actin filaments is partly determined by the spatiotemporal activation of the Rho GTPases. Our formin inhibition data may suggest that EB2 downregulation is associated with formin activation. The perpendicular actin bundles in the EB2-depleted cells resemble Rac1 induced dorsal/radial filaments associated with lamellipodia that are assembled by mDia2. Interestingly, activation of the mDia pathway can lead to Rac1 activation (Kovac et al., 2013; Oakes et al., 2012; Ryu et al., 2009; Tsuji et al., 2002; Yang et al., 2007). Alternatively, the balance between Arp2/3 nucleated actin networks and formin activated linear actin cables or bundles may be shifted towards formin induced actin filament assembly and thus perpendicular actin bundles emanating from the cortex become prominent. In confluent and apico-basal polarising epithelial cells localised activation of junction located formin could trigger nucleation of actin bundles and initiate microtubule–actin filament co-alignment, a process most likely facilitated by ACF7 (Kodama et al., 2003). This is supported by our data on formin inhibition in EB2-depleted cells, which rescued the control phenotype inducing loss of microtubule–actin filament co-alignment and microtubule-associated ACF7 in EB2-depleted cells.

Diaphanous formins bind microtubules directly via their FH2 domain and are also known to stabilise microtubules (Bartolini and Gundersen, 2010; Thurston et al., 2012). EB1 binds to mDia and has been suggested to function downstream of Rho and mDia (Bartolini and Gundersen, 2010; Palazzo et al., 2001; Wen et al., 2004). Here we show that formin inhibition with SMIFH2 in EB2

depleted cells resulted in decreased EB1 lattice association. This suggests that EB1 may need to interact with formin in order to bind along the microtubule lattice or that formin-induced microtubule stabilisation facilitates EB1 lattice binding. Repulsive forces due to negative charges between the C-terminus of EB1 and the microtubule surface has been suggested to favour EB1 binding at the plus-end (Buey et al., 2011). It will be interesting in the future to determine whether formin binding to EB1 or microtubules reduces the repulsive forces and thus makes EB1 lattice association more favourable. A combination of increased GTP–tubulin within the microtubule lattice and reduced repulsive forces may thus facilitate EB1 lattice binding.

The precise temporal and spatial expression of EB2 and EB1 during epithelial differentiation is evidently critical for apico-basal microtubule bundle formation and epithelial differentiation. EB2 expression and binding along the length of microtubules, as particularly evident in the stem cell region of the crypt, for example, may prevent EB1 formin interaction, lattice binding and bundle formation and thus maintain a dynamic microtubule population. The fact that overexpression of EB2 does not induce microtubule bundles, while EB1 does, supports this idea (Bu and Su, 2001). EB1 depletion during epithelial differentiation did not prevent initial microtubule reorganisation and cell constriction possibly due to compensation by EB3 as shown by our double depletion studies of EB2 and EB1. However, lack of EB1 did inhibit apico-basal microtubule bundle formation suggesting that although EB3 can associate along the microtubule lattice it can not fully compensate for EB1's role in apico-basal bundle formation.

Here our findings suggest a model for apico-basal bundle formation dependent on EB2 expression levels. EB2 expression at early stages of differentiation maintains a dynamic microtubule population important for cell–cell junction formation, apical localisation of Rho effectors and activation of Rho/ROCK/myosinII for apical constriction and for initial microtubule reorganisation. Subsequent EB2 downregulation favours formin mediated actin filament assembly, microtubule stabilisation and co-alignment with actin filaments and EB1 and ACF7 lattice recruitment. We propose that EB1 and ACF7 lattice association play a dual role in guiding and cross-linking microtubules to formin nucleated linear actin bundles resulting in the generation of stable apico-basal bundles and that this process is dependent on the downregulation of EB2 (Fig. 10B).

Materials and Methods

Cell culture and drug treatment

Cells lines were maintained at 37℃ in 5% CO^2 and passaged twice weekly. ARPE-19 cells (human retinal pigment epithelial) and mIMCD-3 (inner medullary collecting duct) cells were cultured in DMEM/F12 containing 5 mM Hepes, 2% sodium bicarbonate and 2.5 mM L-glutamine (Invitrogen) supplemented with 10% FBS. TC7 (sub-clone of human colorectal adenocarcinoma cell line Caco-2), U2OS (human Osteosarcoma) and HCT-116 (human colorectal cancer) cells were cultured in DMEM (Invitrogen) containing 10% FBS, 1% L-glutamine and 0.1 mg/ml streptomycin and 100 units/ml penicillin. mIMCD-3 and TC7 cells were grown on 0.4 μm pore polycarbonate cell culture inserts (Nunc) for 5–7 days to stimulate epithelial polarisation. For differentiation analysis mIMCD-3 cells were seeded at 0.24×10^4 cells in 6-well plates and were fixed and lysed every other day for 12 days. For cold treatment analysis ARPE-19 cells were incubated on ice for 90 minutes. Microtubule stability was induced in the ARPE-19 cells by treatment with 2 μM of Taxol (Sigma) for 12 hours. For ROCK inhibition ARPE-19 cells were treated with either 10 μM or 30 μM of Y27632 (Tocris) for 24 hours. Formin inhibition was performed in ARPE-19 cells and cells were treated with 10 μM of SMIFH2 (Sigma) for 40 minutes, a DMSO control was used for each treatment.

Immunolabelling and tissue isolation

Fixation and immunolabelling of cultured cells were performed as previously described (Bellett et al., 2009). Rabbit polyclonal antibodies against ACF7 (HPA013713 Sigma), α-tubulin (ab15246 Abcam) and Ki-67 (Leica Microsystems) were used at 1:100, antibodies against detyrosinated tubulin (ab48389 Abcam) and β-actin (ab8227 Abcam) at 1:200 and antibodies against EB1 (ab50188 Abcam) at 1:2000. Mouse monoclonal antibodies against EB1 (BD biosciences) were used at 1:500. Rat monoclonal antibodies against EB2 clone k52 (Abcam) and EB3 clone KT36 (Abcam) were used at 1:200 and antibodies against tyrosinated tubulin clone YL1/2 (Abcam) at 1:1000. For actin staining phalloidin conjugated to AlexaFluor 488 (Invitrogen) was used at 1:200. Secondary antibodies conjugated to AlexaFluor 488, 568, or 647 (Invitrogen) were used at 1:1000. For isolated tissue staining highly cross-absorbed secondary antibodies conjugated to Dylight 488 and 647 (Jackson) were used at 1:800.

Organ of corti isolation and immunolabelling was performed as previously described (Mogensen et al., 2000). Small intestine and colon was fractioned as previously described (Belshaw et al., 2010; Whitehead et al., 1993). Isolated fractions were fixed in cold −20℃ methanol for 10 minutes and stained as above.

SDS PAGE and immunoblotting

Cells were lysed in lysis buffer (50 mM Hepes, 50 mM NaCl, 1 mM EDTA, 10% Glycerol, 1% TritonX100, 1 mM PMSF, 10 μg/ml aprotinin) at 4℃. Equal proteins concentration was determined using a BCA assay (Pierce) and samples were run using SDS PAGE. Proteins were transferred onto nitrocellulose membrane (BioRad), which was blocked in PBS-T [PBS containing 0.5% milk powder (oxoid) and 0.05% Tween20] overnight at 4℃. The membrane was probed for primary antibodies diluted as indicated in PBS-T. Rabbit polyclonal antibodies against β-actin were used at 1:10,000, α-tubulin and detyrosinated tubulin at 1:500. Mouse monoclonal antibodies against EB1 and RFP (ab65856 Abcam) were used at 1:500 and 1:1000 respectively. Rat polyclonal antibodies against EB2 clone K52 were used at 1:200. The membrane was washed and then incubated with secondary HRP-conjugated antibodies (Sigma) used at 1:10,000. For reprobing, membranes were stripped (Chemicon) and antibody incubation and detection was repeated.

RNAi transfection

ARPE-19, HCT-116 and U2OS cells were treated with 27 nM of siRNA (Qiagen) whereas TC7 cells were treated with 72 nM of siRNA. All siRNA was delivered by Oligofectamine (Invitrogen) as per manufacturer's protocol at indicated timepoints. For negative controls Allstar scramble siRNA sequence (Qiagen) was used. Human EB1 target sequence ACCAATTGCATCCCAGCTAAA. Human EB2 siRNA target sequences; EB2 siRNA (a) CAGCAGGTGC-AGCTAAARCAA, EB2 siRNA (b) AACGCAGGTCATACAGCTTAA, EB2 siRNA (c) GACCTTATTAATAGGAGCATA, EB2 siRNA (d) CTCGATAACC-CAAGAGACTAT. For simultaneous depletion of EB1 and EB2 mRNA, ARPE-19 cells were treated with 54 nM of siRNA (27 nM of each siRNA) at 0 hours and 48 hours.

For ARPE-19 cell size analysis; cells were grown to confluence and the area of 310 control, scramble and EB2-depleted cells and 55 rescued cells were measured blindly. For cell proliferation analysis ARPE-19 cells were seeded at 0.1×10^6 per well (multiwall plate, 6) before each siRNA treatment (0 and 48 hours) and cell population was measured 24 hours and 48 hours later. For apico-basal array analysis, TC7 cells were treated with siRNA at 0 hours, 48 hours and 96 hours. At 102 hours cells were seeded at 0.3×10^6 onto coverslips in 24-well plates and left for a further 42 hours before fixation/lysis.

mCherry–EB2 generation and cDNA transfection

EB2 cDNA was cloned from mIMCD-3 cells using Expand High Fidelity PCR System (Roche). Primers based on NM_001162942 were designed in frame and with restriction sites for cloning into the pmCherry-C1 vector (Clontech). The insert was restricted by *Xho*I and *Hin*dIII (Roche), purified by gel extraction (Qiagen), and ligated using T4 DNA Ligase (Amersham Biosciences) into pmCherry-C1. For transient transfection jetPRIME (Polyplus) was used according to manufacturer's protocol to deliver 2 μgs of mCherry–EB2 cDNA into ARPE-19 cells for overexpression and rescue experiments.

Widefield, confocal and electron microscopy

Electron microscopy was performed as previously described in Bellett et al. (Bellett et al., 2009). Fixed and immunolabelled cells were imaged on a widefield upright Zeiss Axiovert 200M microscope. Images were taken using a monochrome CCD camera and processed using Axiovision (Zeiss) and Photoshop (Adobe) software. Polarised cells and isolated tissues were imaged using a Zeiss LSM510 META scanning confocal microscope. Images were taken using Zeiss LSM software and processed using Volocity (Improvision) and Photoshop (Adobe) software. For live microscopy cells were maintained on a heated stage at 37℃ with 5% CO^2. For analysis of cell division, scramble and EB2-siRNA-treated ARPE-19 cells were grown in six-well plates and phase contrast images were captured using a ×20 objective every 10 minutes for a 24 hour period, beginning at 72 hours after

siRNA treatment. For analysis of microtubule dynamics, untreated, scramble and EB2-siRNA-treated ARPE-19 cells stably expressing GFP–α-tubulin (Clontech) were maintained in phenol red free DMEM/F12 (Invitrogen) medium supplemented with 10% FBS (Invitrogen), 2.5 mM L-glutamine (Invitrogen), 5 mM Hepes and 2% sodium bicarbonate (Invitrogen), in a 3 cm glass-bottomed Petri dish (MatTek), 96 hours after siRNA treatment. Images were captured at set exposure levels using a ×63 objective every 3 seconds for 3 minutes. 12.5×12.5 µm areas were selected and processed in FIJI (Image J) software; briefly, areas were treated with the unsharp mask filter, smoothed, inverted and the brightness and contrast adjusted. Microtubule length in each frame was manually measured in FIJI. Individual frames were annotated in Adobe Photoshop, and assembled into movies using Time-lapse (Microprojects). Adobe illustrator CS6 was used for final figure production.

Statistical analysis

A two-tailed unpaired *t*-test with Welch's correction was used to determine statistical significance for cell area analysis of EB2 siRNA in ARPE-19 cells. Cell height and size of differentiating TC7 was measured and averaged from boxed regions (143 µm×143 µm). Multiple regions were then further averaged for each treatment and statistical significance was determined using a two-tailed unpaired *t*-test. For fluorescence intensity analysis of EB1 and ACF7 along the microtubule lattice, average intensity along 2 µm sections of 25 random microtubules (using tubulin channel) was measured from set exposure images (from the same experiment) using AndorIQ (Andor), statistical significance was determined using a two-tailed unpaired *t*-test. Microtubule dynamics were analysed using length between frames, where movements $\geq \pm 0.5$ µm (width of fluorescence of microtubule) were scored as growth or shrinkage. For each microtubule the percentage of time spent growing, shrinking and pausing was calculated. Using a two-tailed unpaired *t*-test statistical significance was determined from data averaged from five cells (total of 60+ microtubules per treatment). To assess microtubule straightness the average number of microtubule crossover events in cortical 10 µm×10 µm boxes were counted in five cells (three boxes per cell) for each experiment ($n=3$) and significance was determined using a two tailed unpaired *t*-test. For cell proliferation assessment cell growth and Ki-67 expression was analysed using a two-tailed unpaired *t*-test. Summaries of data and significance can be found in supplementary material Table S1.

Acknowledgements

The authors wish to thank James Perkins for help with tissue culture, Richard Evans-Gowing for help with Electron Microscopy, Selina Catto for help with diagrams, Uli Mayer for advice and Paul Wright for IT assistance. We also thank Alan Prescott for helpful discussions and Jelena Gavrilovic and Jeremy Hyams for helpful discussions and comments on the manuscript.

Author contributions

D.A.G., J.R.G., G.B. and M.M.M. conceived and designed the experiments. D.A.G., J.R.G. and G.B. performed experiments and analysed data. D.A.G. and J.R.G. assisted with figure preparations and D.A.G. with writing the manuscript. J.K. and B.J.T. assisted with design and performance of experiments. P.P.P. and E.K.L. provided expertise and training in construct work and crypt isolation respectively. P.T. provided expertise and assistance with microscope imaging and analyses. M.M.M. analysed data, directed the project and wrote the manuscript. All authors read and edited the manuscript.

Funding

This project was supported by the Biotechnology and Biological Sciences Research Council (BBSRC) [grant numbers BB/D012201\1 to M.M.M. and G.B.; BB/J009040/1 to M.M.M. and D.A.G.; and BBS/B/00689 to P.P.P.]; the Anatomical Society (AS) (studentship support to D.A.G.); the BigC Appeal (Studentship supports to J.R.G. and J.K.); and the BBSRC (Studentship support to B.J.T.).

Supplementary material available online at
http://jcs.biologists.org/lookup/suppl/doi:10.1242/jcs.129759/-/DC1

References

Alves-Silva, J., Sánchez-Soriano, N., Beaven, R., Klein, M., Parkin, J., Millard, T. H., Bellen, H. J., Venken, K. J., Ballestrem, C., Kammerer, R. A. et al. (2012). Spectraplakins promote microtubule-mediated axonal growth by functioning as structural microtubule-associated proteins and EB1-dependent +TIPs (tip interacting proteins). *J. Neurosci.* **32**, 9143-9158.

Bacallao, R., Antony, C., Dotti, C., Karsenti, E., Stelzer, E. H. and Simons, K. (1989). The subcellular organization of Madin-Darby canine kidney cells during the formation of a polarized epithelium. *J. Cell Biol.* **109**, 2817-2832.

Bane, B. C., MacRae, T. H., Xiang, H., Bateman, J. and Slepecky, N. B. (2002). Microtubule cold stability in supporting cells of the gerbil auditory sensory epithelium: correlation with tubulin post-translational modifications. *Cell Tissue Res.* **307**, 57-67.

Bartolini, F. and Gundersen, G. G. (2010). Formins and microtubules. *Biochim. Biophys. Acta* **1803**, 164-173.

Bellett, G., Carter, J. M., Keynton, J., Goldspink, D., James, C., Moss, D. K. and Mogensen, M. M. (2009). Microtubule plus-end and minus-end capture at adherens junctions is involved in the assembly of apico-basal arrays in polarised epithelial cells. *Cell Motil. Cytoskeleton* **66**, 893-908.

Belshaw, N. J., Pal, N., Tapp, H. S., Dainty, J. R., Lewis, M. P., Williams, M. R., Lund, E. K. and Johnson, I. T. (2010). Patterns of DNA methylation in individual colonic crypts reveal aging and cancer-related field defects in the morphologically normal mucosa. *Carcinogenesis* **31**, 1158-1163.

Bu, W. and Su, L. K. (2001). Regulation of microtubule assembly by human EB1 family proteins. *Oncogene* **20**, 3185-3192.

Bu, W. and Su, L. K. (2003). Characterization of functional domains of human EB1 family proteins. *J. Biol. Chem.* **278**, 49721-49731.

Buey, R. M., Mohan, R., Leslie, K., Walzthoeni, T., Missimer, J. H., Menzel, A., Bjelic, S., Bargsten, K., Grigoriev, I., Smal, I. et al. (2011). Insights into EB1 structure and the role of its C-terminal domain for discriminating microtubule tips from the lattice. *Mol. Biol. Cell* **22**, 2912-2923.

Chang, Y. C., Nalbant, P., Birkenfeld, J., Chang, Z. F. and Bokoch, G. M. (2008). GEF-H1 couples nocodazole-induced microtubule disassembly to cell contractility via RhoA. *Mol. Biol. Cell* **19**, 2147-2153.

Cheng, I. K., Tsang, B. C., Lai, K. P., Ching, A. K., Chan, A. W., To, K. F., Lai, P. B. and Wong, N. (2012). GEF-H1 over-expression in hepatocellular carcinoma promotes cell motility via activation of RhoA signalling. *J. Pathol.* **228**, 575–585.

Darenfed, H., Dayanandan, B., Zhang, T., Hsieh, S. H., Fournier, A. E. and Mandato, C. A. (2007). Molecular characterization of the effects of Y-27632. *Cell Motil. Cytoskeleton* **64**, 97-109.

des Georges, A., Katsuki, M., Drummond, D. R., Osei, M., Cross, R. A. and Amos, L. A. (2008). Mal3, the Schizosaccharomyces pombe homolog of EB1, changes the microtubule lattice. *Nat. Struct. Mol. Biol.* **15**, 1102-1108.

Dimitrov, A., Quesnoit, M., Moutel, S., Cantaloube, I., Poüs, C. and Perez, F. (2008). Detection of GTP-tubulin conformation in vivo reveals a role for GTP remnants in microtubule rescues. *Science* **322**, 1353-1356.

Furness, D. N., Hackney, C. M. and Steyger, P. S. (1990). Organization of microtubules in cochlear hair cells. *J. Electron Microsc. Tech.* **15**, 261-279.

Gao, S. Y., Li, C. Y., Chen, J., Pan, L., Saito, S., Terashita, T., Saito, K., Miyawaki, K., Shigemoto, K., Mominoki, K. et al. (2004). Rho-ROCK signal pathway regulates microtubule-based process formation of cultured podocytes—inhibition of ROCK promoted process elongation. *Nephron. Exp. Nephrol.* **97**, e49-e61.

Gasteier, J. E., Schroeder, S., Muranyi, W., Madrid, R., Benichou, S. and Fackler, O. T. (2005). FHOD1 coordinates actin filament and microtubule alignment to mediate cell elongation. *Exp. Cell Res.* **306**, 192-202.

Gerdes, J., Lemke, H., Baisch, H., Wacker, H. H., Schwab, U. and Stein, H. (1984). Cell cycle analysis of a cell proliferation-associated human nuclear antigen defined by the monoclonal antibody Ki-67. *J. Immunol.* **133**, 1710-1715.

Gierke, S. and Wittmann, T. (2012). EB1-recruited microtubule +TIP complexes coordinate protrusion dynamics during 3D epithelial remodeling. *Curr. Biol.* **22**, 753-762.

Ishizaki, T., Morishima, Y., Okamoto, M., Furuyashiki, T., Kato, T. and Narumiya, S. (2001). Coordination of microtubules and the actin cytoskeleton by the Rho effector mDia1. *Nat. Cell Biol.* **3**, 8-14.

Kadir, S., Astin, J. W., Tahtamouni, L., Martin, P. and Nobes, C. D. (2011). Microtubule remodelling is required for the front-rear polarity switch during contact inhibition of locomotion. *J. Cell Sci.* **124**, 2642-2653.

Karakesisoglou, I., Yang, Y. and Fuchs, E. (2000). An epidermal plakin that integrates actin and microtubule networks at cellular junctions. *J. Cell Biol.* **149**, 195-208.

Kobielak, A., Pasolli, H. A. and Fuchs, E. (2004). Mammalian formin-1 participates in adherens junctions and polymerization of linear actin cables. *Nat. Cell Biol.* **6**, 21-30.

Kodama, A., Karakesisoglou, I., Wong, E., Vaezi, A. and Fuchs, E. (2003). ACF7: an essential integrator of microtubule dynamics. *Cell* **115**, 343-354.

Komarova, Y., Lansbergen, G., Galjart, N., Grosveld, F., Borisy, G. G. and Akhmanova, A. (2005). EB1 and EB3 control CLIP dissociation from the ends of growing microtubules. *Mol. Biol. Cell* **16**, 5334-5345.

Komarova, Y., De Groot, C. O., Grigoriev, I., Gouveia, S. M., Munteanu, E. L., Schober, J. M., Honnappa, S., Buey, R. M., Hoogenraad, C. C., Dogterom, M. et al. (2009). Mammalian end binding proteins control persistent microtubule growth. *J. Cell Biol.* **184**, 691-706.

Kovac, B., Teo, J. L., Mäkelä, T. P. and Vallenius, T. (2013). Assembly of non-contractile dorsal stress fibers requires α-actinin-1 and Rac1 in migrating and spreading cells. *J. Cell Sci.* **126**, 263-273.

Krendel, M., Zenke, F. T. and Bokoch, G. M. (2002). Nucleotide exchange factor GEF-H1 mediates cross-talk between microtubules and the actin cytoskeleton. *Nat. Cell Biol.* **4**, 294-301.

Lansbergen, G. and Akhmanova, A. (2006). Microtubule plus end: a hub of cellular activities. *Traffic* **7**, 499-507.

Li, W., Miki, T., Watanabe, T., Kakeno, M., Sugiyama, I., Kaibuchi, K. and Goshima, G. (2011). EB1 promotes microtubule dynamics by recruiting Sentin in Drosophila cells. *J. Cell Biol.* **193**, 973-983.

Maurer, S. P., Bieling, P., Cope, J., Hoenger, A. and Surrey, T. (2011). GTPgammaS microtubules mimic the growing microtubule end structure recognized by end-binding proteins (EBs). *Proc. Natl. Acad. Sci. USA* **108**, 3988-3993.

Maurer, S. P., Fourniol, F. J., Bohner, G., Moores, C. A. and Surrey, T. (2012). EBs recognize a nucleotide-dependent structural cap at growing microtubule ends. *Cell* **149**, 371-382.

Mogensen, M. M., Malik, A., Piel, M., Bouckson-Castaing, V. and Bornens, M. (2000). Microtubule minus-end anchorage at centrosomal and non-centrosomal sites: the role of ninein. *J. Cell Sci.* **113**, 3013-3023.

Mogensen, M. M., Tucker, J. B., Mackie, J. B., Prescott, A. R. and Näthke, I. S. (2002). The adenomatous polyposis coli protein unambiguously localizes to microtubule plus ends and is involved in establishing parallel arrays of microtubule bundles in highly polarized epithelial cells. *J. Cell Biol.* **157**, 1041-1048.

Morrison, E. E., Wardleworth, B. N., Askham, J. M., Markham, A. F. and Meredith, D. M. (1998). EB1, a protein which interacts with the APC tumour suppressor, is associated with the microtubule cytoskeleton throughout the cell cycle. *Oncogene* **17**, 3471-3477.

Moss, D. K., Bellett, G., Carter, J. M., Liovic, M., Keynton, J., Prescott, A. R., Lane, E. B. and Mogensen, M. M. (2007). Ninein is released from the centrosome and moves bi-directionally along microtubules. *J. Cell Sci.* **120**, 3064-3074.

Nakata, T., Niwa, S., Okada, Y., Perez, F. and Hirokawa, N. (2011). Preferential binding of a kinesin-1 motor to GTP-tubulin-rich microtubules underlies polarized vesicle transport. *J. Cell Biol.* **194**, 245-255.

Oakes, P. W., Beckham, Y., Stricker, J. and Gardel, M. L. (2012). Tension is required but not sufficient for focal adhesion maturation without a stress fiber template. *J. Cell Biol.* **196**, 363-374.

Palazzo, A. F., Cook, T. A., Alberts, A. S. and Gundersen, G. G. (2001). mDia mediates Rho-regulated formation and orientation of stable microtubules. *Nat. Cell Biol.* **3**, 723-729.

Pepperkok, R., Bré, M. H., Davoust, J. and Kreis, T. E. (1990). Microtubules are stabilized in confluent epithelial cells but not in fibroblasts. *J. Cell Biol.* **111**, 3003-3012.

Rizvi, S. A., Neidt, E. M., Cui, J., Feiger, Z., Skau, C. T., Gardel, M. L., Kozmin, S. A. and Kovar, D. R. (2009). Identification and characterization of a small molecule inhibitor of formin-mediated actin assembly. *Chem. Biol.* **16**, 1158-1168.

Ryu, J. R., Echarri, A., Li, R. and Pendergast, A. M. (2009). Regulation of cell-cell adhesion by Abi/Diaphanous complexes. *Mol. Cell. Biol.* **29**, 1735-1748.

Sandblad, L., Busch, K. E., Tittmann, P., Gross, H., Brunner, D. and Hoenger, A. (2006). The Schizosaccharomyces pombe EB1 homolog Mal3p binds and stabilizes the microtubule lattice seam. *Cell* **127**, 1415-1424.

Scaife, R. M., Job, D. and Langdon, W. Y. (2003). Rapid microtubule-dependent induction of neurite-like extensions in NIH 3T3 fibroblasts by inhibition of ROCK and Cbl. *Mol. Biol. Cell* **14**, 4605-4617.

Siegrist, S. E. and Doe, C. Q. (2007). Microtubule-induced cortical cell polarity. *Genes Dev.* **21**, 483-496.

Shannon, K. B., Canman, J. C., Ben Moree, C., Tirnauer, J. S. and Salmon, E. D. (2005). Taxol-stabilized microtubules can position the cytokinetic furrow in mammalian cells. *Mol Biol Cell* **16**, 4423-4436.

Slepecky, N. B., Henderson, C. G. and Saha, S. (1995). Post-translational modifications of tubulin suggest that dynamic microtubules are present in sensory cells and stable microtubules are present in supporting cells of the mammalian cochlea. *Hear. Res.* **91**, 136-147.

Straube, A. and Merdes, A. (2007). EB3 regulates microtubule dynamics at the cell cortex and is required for myoblast elongation and fusion. *Curr. Biol.* **17**, 1318-1325.

Su, L. K. and Qi, Y. (2001). Characterization of human MAPRE genes and their proteins. *Genomics* **71**, 142-149.

Su, L. K., Burrell, M., Hill, D. E., Gyuris, J., Brent, R., Wiltshire, R., Trent, J., Vogelstein, B. and Kinzler, K. W. (1995). APC binds to the novel protein EB1. *Cancer Res.* **55**, 2972-2977.

Szarama, K. B., Stepanyan, R., Petralia, R. S., Gavara, N., Frolenkov, G. I., Kelley, M. W. and Chadwick, R. S. (2012). Fibroblast growth factor receptor 3 regulates microtubule formation and cell surface mechanical properties in the developing organ of Corti. *Bioarchitecture* **2**, 214-219.

Takesono, A., Heasman, S. J., Wojciak-Stothard, B., Garg, R. and Ridley, A. J. (2010). Microtubules regulate migratory polarity through Rho/ROCK signaling in T cells. *PLoS ONE* **5**, e8774.

Tassin, A. M., Maro, B. and Bornens, M. (1985). Fate of microtubule-organizing centers during myogenesis in vitro. *J. Cell Biol.* **100**, 35-46.

Thurston, S. F., Kulacz, W. A., Shaikh, S., Lee, J. M. and Copeland, J. W. (2012). The ability to induce microtubule acetylation is a general feature of formin proteins. *PLoS ONE* **7**, e48041.

Tirnauer, J. S. and Bierer, B. E. (2000). EB1 proteins regulate microtubule dynamics, cell polarity, and chromosome stability. *J. Cell Biol.* **149**, 761-766.

Tsuji, T., Ishizaki, T., Okamoto, M., Higashida, C., Kimura, K., Furuyashiki, T., Arakawa, Y., Birge, R. B., Nakamoto, T., Hirai, H. et al. (2002). ROCK and mDia1 antagonize in Rho-dependent Rac activation in Swiss 3T3 fibroblasts. *J. Cell Biol.* **157**, 819-830.

Tucker, J. B., Paton, C. C., Richardson, G. P., Mogensen, M. M. and Russell, I. J. (1992). A cell surface-associated centrosomal layer of microtubule-organizing material in the inner pillar cell of the mouse cochlea. *J. Cell Sci.* **102**, 215-226.

van der Flier, L. G. and Clevers, H. (2009). Stem cells, self-renewal, and differentiation in the intestinal epithelium. *Annu. Rev. Physiol.* **71**, 241-260.

van der Vaart, B., Akhmanova, A. and Straube, A. (2009). Regulation of microtubule dynamic instability. *Biochem. Soc. Trans.* **37**, 1007-1013.

Vitre, B., Coquelle, F. M., Heichette, C., Garnier, C., Chrétien, D. and Arnal, I. (2008). EB1 regulates microtubule dynamics and tubulin sheet closure in vitro. *Nat. Cell Biol.* **10**, 415-421.

Wang, F., Zhang, Q., Cao, J., Huang, Q. and Zhu, X. (2008). The microtubule plus end-binding protein EB1 is involved in Sertoli cell plasticity in testicular seminiferous tubules. *Exp. Cell Res.* **314**, 213-226.

Wen, Y., Eng, C. H., Schmoranzer, J., Cabrera-Poch, N., Morris, E. J., Chen, M., Wallar, B. J., Alberts, A. S. and Gundersen, G. G. (2004). EB1 and APC bind to mDia to stabilize microtubules downstream of Rho and promote cell migration. *Nat. Cell Biol.* **6**, 820-830.

Whitehead, R. H., VanEeden, P. E., Noble, M. D., Ataliotis, P. and Jat, P. S. (1993). Establishment of conditionally immortalized epithelial cell lines from both colon and small intestine of adult H-2Kb-tsA58 transgenic mice. *Proc. Natl. Acad. Sci. USA* **90**, 587-591.

Wu, X., Kodama, A. and Fuchs, E. (2008). ACF7 regulates cytoskeletal-focal adhesion dynamics and migration and has ATPase activity. *Cell* **135**, 137-148.

Yang, C., Czech, L., Gerboth, S., Kojima, S., Scita, G. and Svitkina, T. (2007). Novel roles of formin mDia2 in lamellipodia and filopodia formation in motile cells. *PLoS Biol.* **5**, e317.

Zhang, T., Zaal, K. J., Sheridan, J., Mehta, A., Gundersen, G. G. and Ralston, E. (2009). Microtubule plus-end binding protein EB1 is necessary for muscle cell differentiation, elongation and fusion. *J. Cell Sci.* **122**, 1401-1409.